Additive Manufacturing of Titanium Alloys for Orthopedic Applications: A Materials Science Viewpoint

Majumdar, Trina; Eisenstein, Neil; Frith, Jess; Cox, Sophie; Birbilis, Nick

DOI:
10.1002/adem.201800172

Review, No. adem.201800172

Title: Additive Manufacturing of Titanium Alloys for Orthopedic Applications: A Materials Science Viewpoint

*Authors: Trina Majumdar, Neil Eisenstein, Jess E. Frith, Sophie C. Cox, Nick Birbilis**

T. Majumdar, Dr. J. Frith, Prof. N. Birbilis
Department of Materials Science and Engineering, Monash University, Clayton, 3800, Victoria, Australia
E-mail: nick.birbilis@monash.edu

N. Eisenstein, Dr. S.C. Cox,
School of Chemical Engineering, University of Birmingham, Edgbaston, B15 2TT, United Kingdom

Keywords: titanium, additive manufacturing, electron beam melting, selective laser melting, orthopedic implants

Abstract

Titanium-based orthopedic implants are increasingly being fabricated using additive manufacturing (AM) processes such as selective laser melting (SLM), direct laser deposition (DLD) and electron beam melting (EBM). These techniques have the potential to not only produce implants with properties comparable to conventionally manufactured implants, but also improve on standard implant models. These models can be customized for individual patients using medical data, and design features, such as latticing, hierarchical scaffolds or features to complement patient anatomy, can be added using AM to produce highly functional patient-anatomy-specific implants. Alloying prospects made possible through AM allow for the production of Ti-based parts with compositions designed to reduce modulus and stress shielding while improving bone fixation and formation. The design-to-process lead time can be drastically shortened using AM and associated post-processing, making possible the production of tailored implants for individual patients. This review examines the process and product characteristics of the three major metallic AM techniques and assesses the potential for these in the increased global uptake of AM in orthopedic implant fabrication.

1. Introduction

Orthopedic surgeries (including joint replacements) are becoming increasingly common, with more than 1,000,000 surgeries estimated to have occurred in the United States in 2015 alone [1]. The demand for orthopedic implants has increased rapidly in the past few decades due to increases in average life spans globally, as well as increases in physical activity among the elderly. Contemporary orthopedic implants, such as those seen in Figure 1., must last for decades as opposed to years, as well as closely approximate and support the area of replacement in terms of mechanical properties and responses to host biology[1–5]. The requirements for implants in different areas vary, for example hip vs knee implants. Thus, a general view will be taken in this manuscript.

Figure 1 Examples of customized implants. These implants were designed using 3D Digital Imaging and Communications in Medicine (DICOMs) and fabricated using AM techniques.

A cement-less orthopedic implant must bond well to bone in the first month following implantation, to ensure that complete osseointegration over the next few months occurs successfully. [3,4]. Osseointegration is defined as a complete linkage between bone and the implant surface, i.e. mechanical interlocking. Full host to implant contact is achieved by the development of anchorage mechanisms that can withstand natural loading. Implant and bone surface features of various sizes become important at different steps of the osseointegration process [6].

Titanium and its alloys are used widely in orthopedic applications, as seen in Figure 1 and 2, due to low cytotoxicity, high mechanical strength and relative biological inertness [7–10]. Pure Ti is a non-ferrous light metal, with a nominal density of 4.51 g/cm^3 and elastic modulus of 115 GPa [11]. Ti undergoes an allotropic transformation at 882ºC, from a body-centered cubic (β phase) structure to a hexagonal close packed (α-phase) structure (below 882 ºC). The phase transformation is accompanied by slight atomic distortion due to the plane transformation, leading to a slight increase in volume when cooling through the transus temperature (882ºC) [12]. Ti is spontaneously passive, reacting with air or aqueous environments to form a protective oxide layer that is typically ~2-7 nm in thickness. This layer is well maintained at normal body pH levels, and is resistant to localized short-term changes in pH occurring due to infection, however, total corrosion resistance is known to decrease over time due to the interplay of various organic and inorganic molecules such as lipopolysaccharides and albumin [9,13].

The elastic modulus of Ti and its common alloys are generally much higher than that of bone. Pure Ti has a modulus of ~120 GPa while cortical bone has a modulus of 10-30 GPa [3]. When Ti-based implants are in contact with bone, this modulus mismatch results in stress shielding [3,4] – cyclic loading and impact forces are borne largely by the implant rather than the host bone, causing the resorption of this ‘unused’ bone. Stress shielding causes interfacial weakening and the formation of wear debris, potentially leading to the requirement for revision surgeries. The biological inertness of Ti-based alloys, as well as their poor wear properties and notch sensitivity compared to other commonly used stainless steels or cobalt-based alloys, remain as hurdles in successful implant osseointegration[14,15]

Present alloy design for orthopedic applications is moving away from Ti alloys containing toxic elements such as Ti-6Al-4V, and towards lower modulus Ti-based alloys. The lower modulus T-alloys are usually typified by the β phase Ti alloys, with important properties summarized in Table 1.

Some of the most promising alloying elements under investigation are niobium (Nb), zirconium (Zr), tantalum (Ta) and strontium (Sr) These are all β-stabilizing elements (allowing alloys to retain the high temperature BCC β phase at room temperature) with similar cytocompatibility to that of Ti [16–19]. To reduce this effect, Ti is commonly alloyed with elements which act as stabilizers for the β phase, thereby reducing the Young's modulus of the material to closer to that of bone. Of such two-phase alloys, Ti-6Al-4V is the most commonly used for orthopedic implants, with aluminum (Al) serving as an α-phase stabilizer and vanadium (V) serving as a β phase stabilizer [11]. Ti-6Al-4V has an allotropic transformation temperature of 990ºC and a solidus temperature of 1605ºC [11,20,21]

Material	Phase types	Fabrication method	Elastic modulus (GPa)	Yield strength (MPa)	Ultimate tensile strength (MPa)	β transus temp-erature (ºC)
Ti-6Al-4V	α + β	Casting	110	850-900	960-970	995
Ti-13Nb-13Zr	α' + β	Casting	79	900	1030	575
Ti-6Al-7Nb	α + β	Casting	105	921	1024	1010
CP Ti (grade 4)	α	Casting	105	692	100	950
Bone	-	-	10-40	-	90-140	-

Table 1. Nominal mechanical properties of common Ti-based alloys used for orthopedic implants [11,22,23]

Two other strategies in reducing stress shielding and improving the osseointegration of orthopedic Ti implants [24] include: (1) the incorporation of porosity or texture into parts to reduce stiffness and

density (either by design or manufacturing method), and (2) the reduction of modulus mismatch through the development of low modulus Ti-alloys; both approaches elaborated below.

Programming porosity into implant designs through scaffolding may improve the speed and efficacy of osseointegration [25,26]. The porosity of cortical bone (i.e. the femur) is approximately 5-30%, while that of cancellous bone is 30-90% [27]. Non-stochastic porous scaffolding in implants modeled on the porosity of various size scales in living bone can act as templates for the initial attachment and growth of bone-forming cells. Nano-porosity is required for molecular transport, waste removal and cell-cell signaling, while micropores are required to allow cell migration and capillary formation. Full vascularization occurs on the macro scale (mm) [28,29]. Bone cell proliferation and differentiation are thought to be positively influenced by surface roughness, with an average surface roughness or groove width below 1 μm being advocated as optimal [30,31] although other groups have suggested that larger surface grooves of up to 50 μm width [32] may be ideal. While there is no consensus on the best surface topography for osteoblastic adhesion and proliferation, it is agreed that the method in which the texture is achieved is as important as the roughness parameter itself, as this affects surface chemistry [31,33] Surface roughness or texture is to date achieved through post-processing techniques upon Ti and its alloys. Complex surface topographies with a wide range of differently sized features are necessary for successful implants [34,35]. These topographies support the entire process of host bone attachment and the formation of a strong bone-implant interface.

These features can be easily investigated, trialed and produced through AM processes as the page to part lead-time is relatively short. There is no need for re-tooling between design iterations, and relatively low amount of material are required to investigate different options for part design. Other global features such as porosity and surface roughness can be systematically varied through

manipulation of the AM fabrication process. The final implant produced for the patient through AM can be greatly customized in a reduced time period, with reduced costs as compared to conventional processes such as casting.

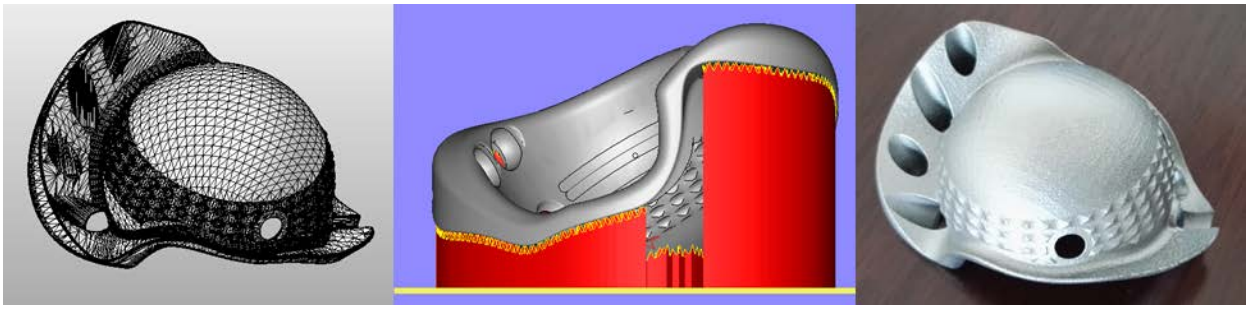

Figure 2 Patient data in the form of computed tomography (CT) or magnetic resonance imaging (MRI) scans can be used to create computer aided design (CAD) models, which can then be used to print custom implants. L-R this figure shows the initial design of a custom implant, the pre-print manipulation of the design including support structures in red and the final post-processed part.

Improving orthopedic implant fabrication and usage via additive manufacturing (AM) techniques offers distinct advantages. Conventional Ti fabrication techniques include near net casting, forging, and machining from wrought ingot and bars. However, as Ti has low thermal conductivity and high reactivity with and affinity for oxygen, this presents difficulties in machining [36,37], and so these methods are often unsuitable for producing implants with patient specific geometries or features. AM processes have already demonstrated an excellent ability to serve as alternative fabrication routes in a number of industries, and as of 2014 the market was estimated to be worth $4.1 billion [38], with Ti and its alloys used for a significant amount of additively manufactured components. The improved geometrical freedom of AM technologies allows for increased complexity and customization. The localized metal melting possible in most AM processes permits for alloying in a manner that bypasses liquid metal (casting) issues such as solute solubility and segregation (and dissimilar melting points, etc.). The alloying freedom of powder-based AM is metallurgically unsurpassable at present. Further benefits of AM include low material wastage and low production

volumes with reduced economy of scale issues[39]. Ultimately, AM allows for the production of parts that were previously un-manufacturable or economically unviable through traditional routes, as per the three-axis model of product manufacturability seen in Figure 3.

Figure 3 The three-axis model of product manufacturability shows that product design must consider complexity, required iterative customizability and required volume to be readily manufacturable.

Reproduced with permission[40] 2014, Elsevier.

In a holistic sense, AM may be carried out through seven major approaches; material extrusion, material jetting, binder jetting, vat photo-polymerization, sheet lamination, directed energy deposition and powder bed fusion, with the latter two used for the fabrication of strong, net shape metallic bone replacements [41]. Powder bed fusion techniques, such as Electron Beam Melting (EBM) and Selective Laser Melting (SLM) utilize either a laser or electron beam to melt and fuse pre-alloyed or pure powders in specified patterns. Direct Laser Deposition (DLD) differs in terms of powder supply - the powder is gravity fed from nozzles into the laser beam and local melt pool. In this way, the powders are sintered into a melt pool on the substrate. Whilst DLD can produce near-net shapes, these have lower tolerances and less complex internal structures than possible through

SLM or EBM. DLD is largely used to produce significantly larger freeform components than either EBM or SLM. In the context of specific implant production, patient scan data, e.g. computed tomography (CT), can be utilized for customized implant designs, which can then be constructed through powder bed fusion or energy deposition methods [39]. This process is visualized in Figure 4.

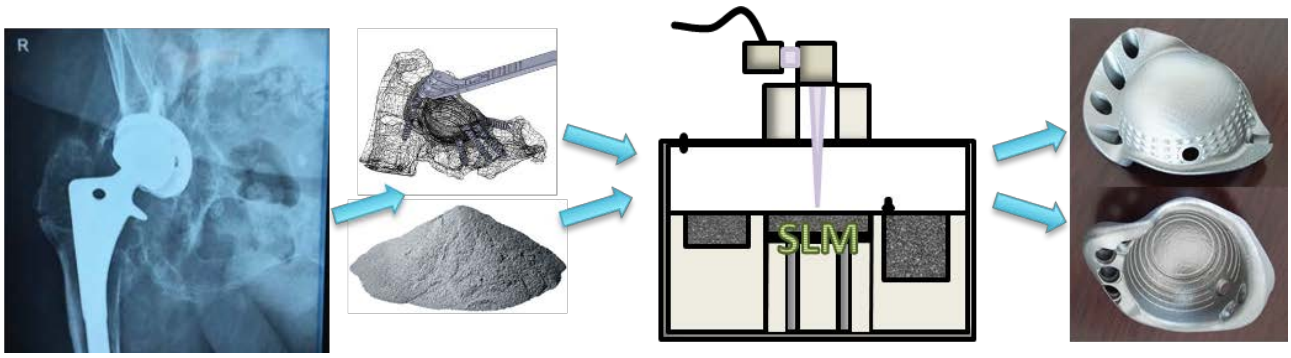

Figure 4 Patients who require custom implants can receive them through the combination of AM techniques and medical imaging. Generally, patient data (e.g. MRI or CT) is used to create the design of the part. This CAD file (in stereolithography format) is sliced and otherwise manipulated such that the AM machine (SLM shown here) can fabricate the part. Following fabrication and some minor post-processing, the custom implant can be delivered to the patient, with a drastically reduced lead time.

Even at this stage of AM development and the commercial availability of production units, work remains to be completed in the full characterization and understanding of AM produced part properties. As with any technique, part fabrication is not as simple as inputting a design and fabricating with fixed settings – care must be taken with the parameters chosen for processing, as each can have a significant effect on the microstructure, build efficiency, and mechanical and implantability-related properties of the part.

The aim of this review is to assess the current research and technology in the context of AM for orthopedic implants, particularly focusing on Ti and its alloys. The first section of this manuscript

examines the major AM techniques currently being used to fabricate Ti implants, as well as process-specific properties as related to Ti-based orthopedic implants, whilst the second and third parts examine pre- and post-fabrication considerations. The fourth section looks at current research being conducted in the area, and the final section will discuss clinical and engineering perspectives on the production of orthopedic implants through AM.

2. Additive manufacturing techniques relevant to orthopedic implants

The three most commonly used AM processes in medical engineering (for orthopedic applications) are SLM, EBM and DLD. Each process begins with the development of a 3D CAD model of the required implant. These models can be made using individual patient data (e.g. from MRI or CT), or from prior (known or standard) designs – this process of applying medical data to a design model can be done through commercial software such as Mimics (Materialise) and Vitrea (Vital Images) [42]. Once the design is complete, it may be further modified to include support structures – these structures act as anchors to the build plate, prevent part warpage due to residual stresses, and aid in heat conduction away from the part. The design can then numerically sliced into 2D layers through the use of software (for example, Magics (Materialise) or Netfabb (Autodesk) [42,43]. The prepared file is sent to the EBM, SLM or DLD machine, where the 3D part is built up through multiple layer-wise deposition and melting stages [39,44,45]. The maximum build volume is specific for each brand of machine, but is generally no larger than 400*400*400mm^3, specifically for SLM and EBM. Following fabrication, the parts are cut away from the build plate and support structures. Post-processing procedures such as hot isostatic pressing (HIPing) and/or stress relieving are performed, followed by surface finishing or polishing as required [46,47]. The part is prepared for implantation through the application of antibacterial or osteo-inductive coatings. Following sterilization (e.g. through γ irradiation), the implant is ready for implantation [48].

The major variables in the SLM and EBM processes are as follows; laser power, layer thickness, scan speed and hatch spacing [45]. These parameters affect the amount of thermal energy supplied to each unit volume of material, the sum of which is termed the energy density (ED). This behavior can be quantified as in Equation 1 [49].

$$E_{density} = \frac{P_{beam}}{v_{scan} \cdot s_{hatching} \cdot t_{layer}} \quad (1)$$

where $E_{density}$ = energy density, P_{laser} = beam power, v_{scan} = scan speed, $s_{hatching}$ = hatch spacing, t_{layer} = layer thickness

Each process produces parts with specific properties, which will be discussed in the following sections. It is important to note that both conventional and AM manufacturing techniques may use the same alloys – however the relationship between processing variables during AM fabrication on part properties (with respect to effects on the human body) is not yet well understood. The bulk of previous research has centered on short term, *in vitro* studies of AM produced parts. A historical view will be taken in the following sections.

2.1 SLM

The main components of SLM machinery, as seen in Figure 5, include a fiber laser (usually Ytterbium) with a beam expander and focusing lenses, a build platform, powder bunker, and powder rake [50]. Pre-alloyed metal powders with average particle diameter between 10 and 45 μm are raked over the build platform, usually pre-heated to between 100 and 200ºC, after which the CAD driven mirror system can direct and focus the laser beam (up to 1 kW) onto the build platform to melt each 2D cross-section into the powder layer. The build table drops down according to the

specified layer thickness, generally between 20 and 100 µm, and another even layer of powder is raked over the work platform. The laser then melts the next layer onto the previous layer [50]. The entire process takes place in a purified nitrogen or argon gas environment to prevent oxidation of the metal powders [24]. The final part is built up by the 'welding' of small overlapping regions, ending in the production of a 3D part with a complex, pulsed thermal history [51].

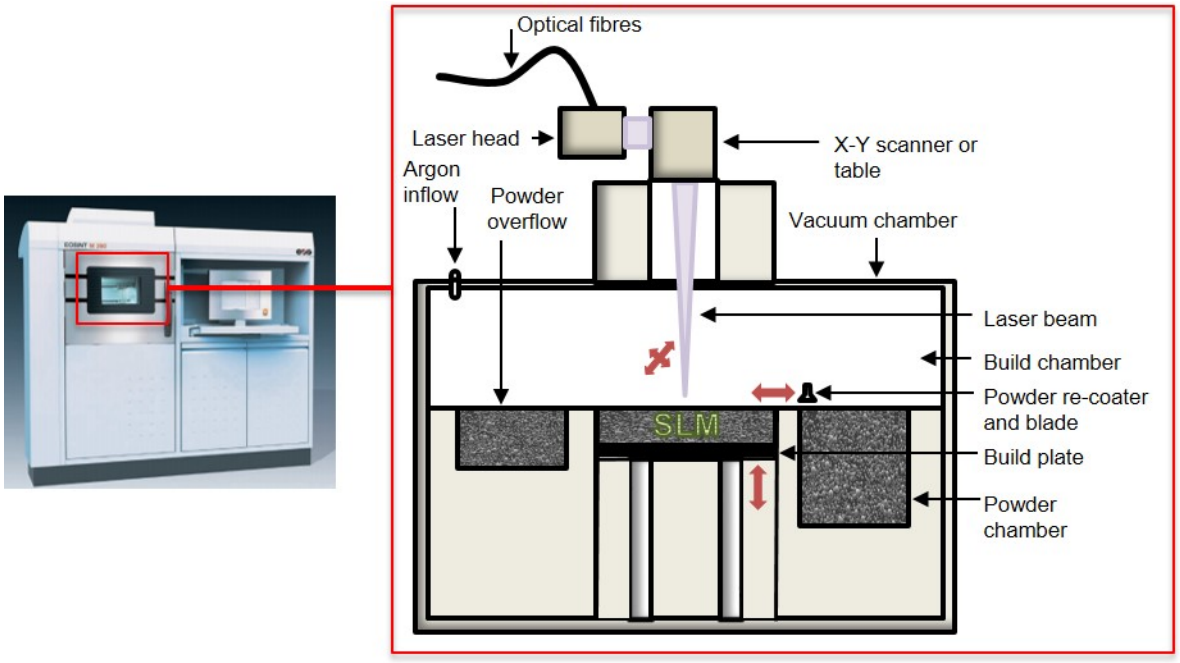

Figure 5 Schematic of SLM Equipment showing fiber laser with, build chamber, powder bunker, powder rake and build-in-progress, and photo of a representative SLM machine.

2.1.1 SLM part properties

SLM characteristically produces parts with complex thermal histories due to the rapid heating and cooling cycles as well as the steep thermal gradients produced across layers [52]. Examples of properties produced by various groups are collected in Table 2 and discussed in the following sections. The laser beam causes localized re-melting and re-cooling cycles adjacent to each scan track. The SLM process inherently produces a steep thermal gradient between the top and bottom surfaces of each layer due to heat transfer through multiple layers. This can lead to melt pool instability, reduction of surface energies as well as dimensional inaccuracies due to contraction on

cooling [24]. Localized re-melting and re-cooling cycles lead to the formation of columnar β phase grains, which are inclined perpendicular to the laser scanning plane [50,53]. These thermal gradients will cause the part to have residual thermal stresses and non-equilibrium phases [54]. Residual stresses must be relieved prior to usage, necessitating post-processing techniques such as stress relieving and/or HIP to reduce the internal stresses and increase the fatigue resistance of parts to that comparable with conventionally fabricated equivalents [52]. Additionally, un-melted or partially melted powder particles may remain on each layer between scans, leading to the formation of micro-voids [55]. Specific part properties are also affected by process parameters and powder characteristics [56].

Taking a closer view, pre-alloyed Ti-6Al-4V powders, with a liquidus temperature of 1650ºC and solidus temperature of 1605ºC, display a "mushy" zone within the melt pool, and the cooling rate of this melt pool informs the layer-wise microstructural progression [57]. Cooling rates within the melt pool can range between 12000 and 40000 ºC/s depending on the amount of energy supplied (dictated by process parameters such as laser power and scan speed) [44,58]. Ti-6Al-4V particles initially solidify into BCC β phase structures, present as both columnar and equiaxed grains. Depending on the cooling rate, the β phase can then transform into α' martensite (above 410ºC/s) or α phase. Taking a macroscopic view, part properties are also spatially dependent due to anisotropic heat removal and interaction of cooling gradients with the bulk un-melted powder surrounding the growing part. The first layer of the part will have a characteristically rough surface finish since it has a reduced thermal conductivity due to it being comprised of loose powder, although this will be further influenced by the method used to cut the part from the substrate, as well as the removal of support structures. This leads to the formation of an unstable melt pool, and stalactite patterns where the cooling melt pool sinks into the adjacent loose powder [45]. The last layer of the part will also have a rough surface finish due to a localized reduction in thermal insulation.

There is a wealth of information regarding the practical capabilities of SLM to produce Ti alloy parts with varying porosities; however, no consensus exists on the minimum or maximum possible pore sizes achievable. Minimum achievable bulk pore sizes have been variously reported as 750 µm [59], 500 µm [60] and 100 µm [61]. SLM part porosities of 31-43% and 32.2 to 53.4% have been achieved by Basalah et al [27] and El-Hajje et al [62] respectively. Guneta et al were able to achieve SLM produced porosities of between 32-53%, however the pore sizes produced were between 17.0-24.0 µm, too small for cells to penetrate into the inner pores[63]. Apart from issues with cell penetration, smaller pore sizes are in any case more difficult to form due to the high local laser power causing the formation of larger melt pools, leading to powder sputtering and pore occlusion [59]. Additionally, issues may arise with depowdering following part completion. Depowdering refers to the process of retrieving the built part from the bulk powder surrounding it, usually through high pressure air blasting, vibratory processing or a combination thereof [44]. Solid parts can be retrieved easily, however, depowdering porous parts is complex [60,64,65], due to instances of weak bonding between layers and loose powder, which can trap powder particles.

SLM parts typically have roughness in the micrometer range, with 2-20 µm representing an average range [66]. This is attributed to thermal gradients across layers, and the staircase effect [45]. Different roughness behavior is observed according to where in the staircase the observed region is (Figure 6). This is due to the presence of partially melted particles remaining on free surfaces. High hardness is also observed due to rapid cooling characteristics and low ductility, generally reported as at least 20% greater than comparable EBM parts [67,68]. Hardness and porosity are interrelated with ED, with a higher energy input causing more complete melting and reduced porosity. The presence of non-equilibrium phases contributes to the higher yield strength of SLM parts as compared to forged parts [45].

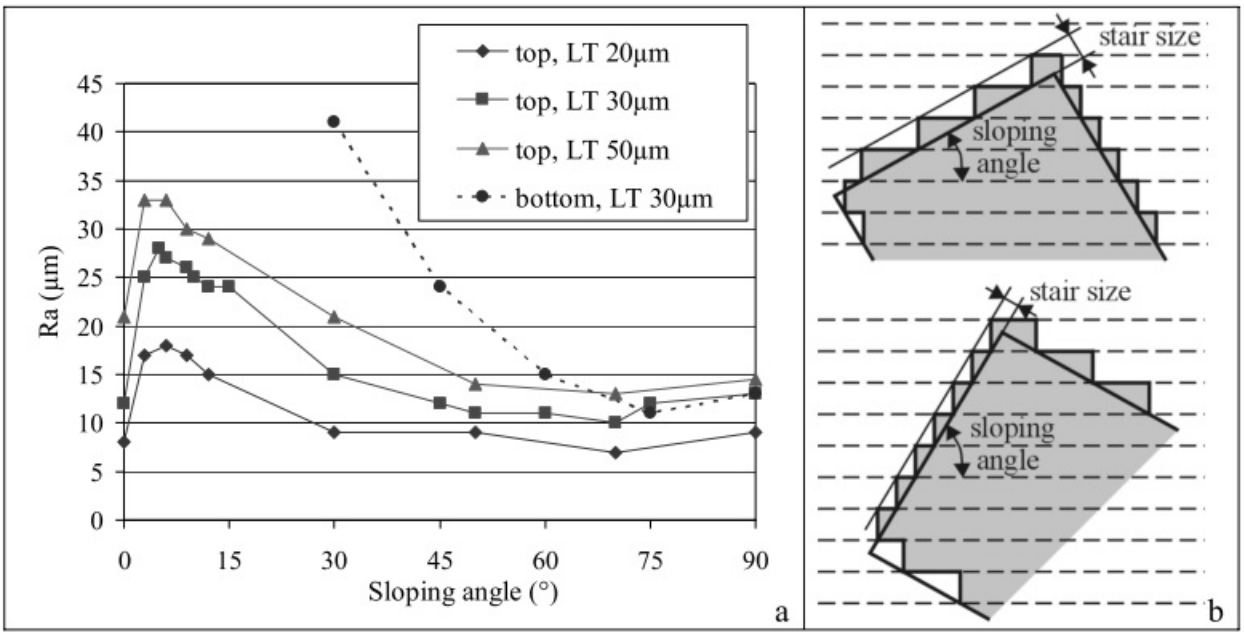

Figure 6 The surface roughness of an SLM produced part can vary significantly according to the surface location when related to a) the printing direction and b) the interaction between sloping angle and layer thickness – 'down-skin' surfaces, or down-facing surfaces show higher surface roughness. This is referred to as the staircase effect.

Reproduced with permission [45] 2007, Elsevier

The major defect types in SLM produced Ti-6Al-4V parts can be classed as follows; un-melted or partially melted particles on surfaces, random porosity and delamination between layers [51,69,70]. Random porosity is generally observed in SLM parts due to the presence of trapped gases in the melt pool, as well as a lack of fusion defects, which occur when there is insufficient ED to completely melt the powders in a small region. This results in the formation of irregularly shaped cavities with un-melted trapped powder particles and is heavily dependent on sinter neck size as well as particle size [27]. These form primarily along interlayer boundaries, and act as local stress concentrators. Micron sized pores affect fatigue strength, while residual stresses can affect fatigue crack growth [52]. SLM produced parts also generally have relatively high oxygen/nitrogen contents

[24]. SLM produced coatings form irregularly shaped particles – the inherent eccentricity of these are key in the formation of porous structures [71].

As mentioned, certain process parameters have been found to affect final product characteristics, the most important of these being scan rate, laser intensity, and layer thickness [72,73]. Changes in scan rate affect microstructural features, with increased scan rates causing the formation of finer dendritic microstructures [74]. This can be attributed to the reduced ratio of temperature gradient to solidification rate, as well as the increased turbulence of melt pools [75]. Increased laser intensity appears to increase density and therefore reduce porosity [76,77]. The increased laser intensity, while creating a larger immediate melt pool, also affects previous layers, resulting in increased heating/cooling cycles – this allows for microstructural refinement in much the same way as increased scan rates.

Key studies into the *in vitro* and *in vivo* behavior of SLM produced Ti-6Al-4V implants include the work of Hollander et al. [78], Warnke et al. [79], Mangano et al. [80], Van Bael et al. [81] and Shaoki et al. [82]. Hollander et al. investigated the behavior of human osteoblasts on annealed sand-blasted SLM produced Ti-6Al-4V over a time period of 14 days [78]. Both porous (200, 400 and 7000 um diameter pores) and non-porous samples were produced, and cell proliferation was found to occur successfully on each of these samples, with proliferation and differentiation (indicated by alkaline phosphatase (ALP) activity) occurring in a manner similar to that expected for wrought Ti-6Al-4V. Following, Warnke et al. investigated the behavior of human osteoblasts (from iliac crest cancellous bone) on mesh Ti-6Al-4V scaffolds over a period of 72 days [79]. In agreement with the work of Hollander et al. (and Van Bael et al.), this experiment showed that pore sizes smaller than 500 µm in diameter result in cell occlusion. This prevents further in-growth and bone regeneration [79]. Cell morphology on the other scaffolds was found to be star-like and well spread, with multiple

filipodial extensions. SLM produced Ti-6Al-4V scaffold biocompatibility was confirmed with the use of lactate dihydrogenase (LDH), 3-(4,5-dimethylthiazol-2-yl)-2, 5-diphenyltetrazolium bromide (MTT), 5-bromo-2- deoxyuridine (BrdU), and water-soluble tetrazolium (WST) tests. The work of Van Bael et al. [81] further showed that lower scaffold permeability led to increased cell attachment. Their work also indicated that cell differentiation is likely to be more affected by pore size (with smaller pores providing more stimuli) than shape. The work of Hollander et al., Warnke et al. and Van Bael et al. all identified one key issue in SLM implant fabrication – actual pore size was often significantly smaller than designed pore size, with the largest diametric variance being 300 µm.

Mangano et al. produced some of the first *in vivo* data for SLM produced implants, by implanting a Ti-6Al-4V mandibular micro-implant into a human patient without complications [80]. This implant was acid etched with oxalic acid and maleic acid to produce a final Ra of 66.8 µm. Retrieval and analysis of this implant after 2 months of healing showed evidence of bone remodeling activity, areas of woven bone and multiple osteocyte lacunae, with a bone-to-implant contact (BIC) percentage of 69.51%. Shaoki et al. compared the *in vivo* performance of SLM-produced Ti-6AL-4V implants with commercially available implants in a canine model, over a period of 9 weeks [82]. Their SLM implant had a higher roughness than the commercial implants (Ra = 10.65 ± 2.3 µm and Ra = 0.33 ± 0.12) but showed no significant differences in bone-implant contact ratio or bone formation, indicating that SLM fabricated Ti-6Al-4V implants are competitive and have great potential for wide spread uptake. More long-term data is yet unavailable.

2.2 EBM

EBM is a powder bed fusion technique quite similar to SLM, with the major difference being the energy source, which is an electron beam as opposed to a laser beam [57,83]. This requires a high vacuum in the build chamber to maintain beam integrity. The powder used in EBM is pre-heated to

40-60% of its melting temperature through successive rapid scans by the electron beam [84]. This is followed by a reduced scanning rate and beam current. The chamber temperature is kept between 650 and 700ºC.

An EBM system contains a computer control/recording section and an electron beam forming and processing system (Figure 7). An electron gun is used to generate an electron beam (up to 3 kW), which is then accelerated through a focusing lens and magnetic scanning coil system [50]. Pre-alloyed metal powders are gravity fed from cassettes and raked evenly over the build table. The focused electron beam is directed by the CAD model slices to selectively melt patterns into the powder layer. The build table is then lowered according to the layer thickness, and the process is repeated until the part is complete. Layer thicknesses for EBM are generally kept at 50 µm, and the average particle size for powders used should be between 45 and 105 µm [85].

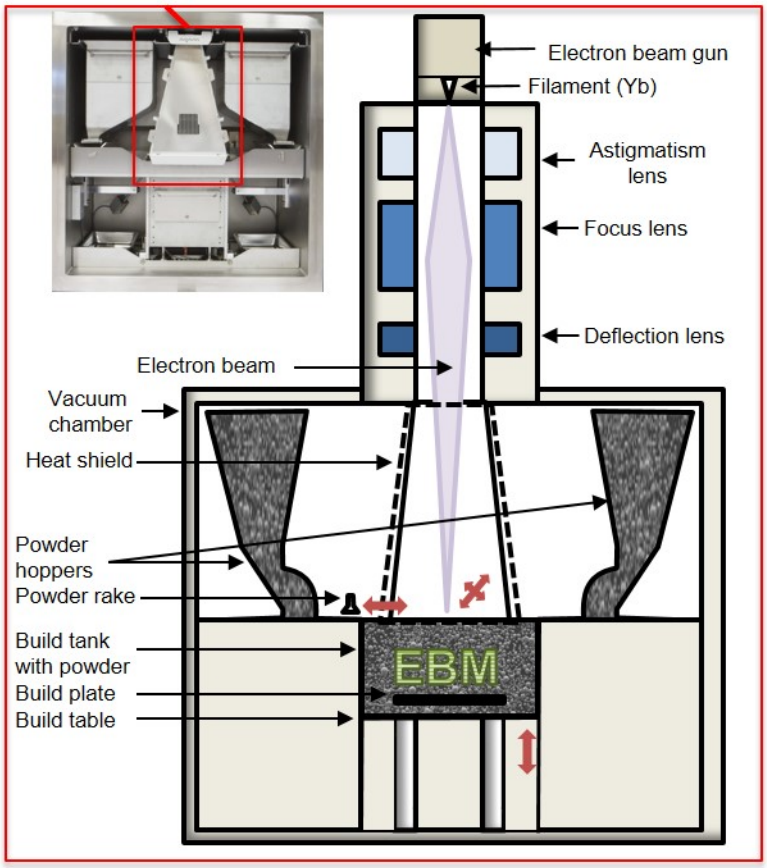

Figure 7 Schematic of EBM machinery showing electron gun assembly, EB focusing lens, EB deflection lens, powder hoppers, powder (layer) rake, build-in-progress, and build table, with photo of representative EBM machine.

EBM has several benefits, particularly for the fabrication of parts comprised of alloys that have a high chemical affinity to atmospheric gases, including Ti, this issue is bypassed in EBM, as the process occurs in a vacuum [86]. The background vacuum is maintained within 10^{-4} to 10^{-5} Torr, with a helium bleed near the build area where the vacuum is reduced to 10^{-2} Torr to aid cooling and beam scan stability [44,87]. The process is extremely energy efficient, due to the high conversion efficiency from electricity to electron beam energy [87]. Almost all of this energy can be absorbed by the material/powder. Thus, the beam will have a large penetration depth, leading to the formation of a high temperature melt pool [88].

2.2.1 EBM part properties

Parts produced through EBM undergo characteristic microstructural progressions [87,89]. During part building, the part microstructure is initially composed of primary β phase. This then transforms to α martensite, which decomposes into α and β phases. This characteristic progression can be seen in Figure 8. The β phase is composed of coarse columnar grains, and therefore EBM parts are highly anisotropic [90]. This occurs as a result of the beam penetration depth being greater than the layer thickness meaning each layer is transformed several times. The uppermost layer, i.e. the layer with lowest thermal insulation, is formed entirely of non-equilibrium α' phase grains. In the bulk, relatively slower cooling allows the α' phase to decompose into α and β phases, leading to closer modulus matching with bone than conventionally manufactured Ti-based alloys.

The surface features produced by EBM are often difficult to control without post processing, and are limited by the spatial resolution of the method [35]. Diffusion between build table substrates and the formed part may be observed, but this can be avoided through the use of a sacrificial support base [87]. Powder blow-away is a common undesirable process feature, which occurs due to electrostatic repulsion between beam and powder [87]. Pre-heating the powder to ~730ºC using a defocused beam, with currents between 28-38 mA, and a scanning rate of 146000 mm/s [91,92], can be done to reduce this. The small-scale sintering occurring during pre-heating can reduce the blow-away of the powder particles. However, post-process powder entrapment still presents a problem [39,88].

Many groups have investigated the mechanical properties and surface behavior of EBM produced Ti-based alloys, and information about these is collated in Table 2. and discussed here. EBM structures have thicker oxide layers than conventionally machined surfaces [36], with the specific thickness of these oxides being dependent on location, as seen in in Figure 8. and 9. This is thought to be due to the presence of oxidative gas species in the vacuum chamber, and the diffusion of oxygen from the bulk of the component to the outer layers, resulting in net oxide growth. Oxide thickness is also dependent on surface – different areas of the growing part will undergo different cooling patterns during manufacture [21,36,91]. Upper layers undergo rapid cooling due to the absence of surrounding material, resulting in thinner oxide layers. In contrast, side surfaces are embedded between adjacent un-melted powder particles, which act as thermal insulators. The high temperatures partially sinter these adjacent particles and vaporize residual moisture in the powder bed. This causes the formation of oxides 50% thicker than those present on the upper surfaces. [91]. Oxide thickness is also affected by build height; larger builds allow for the release of trapped moisture in the chamber, leading to increased stability. The upper surface oxide layer is thus only formed after the temperature of the layer is insufficient to drive oxygen diffusion from the bulk to

the surface. Therefore, the oxide formation characteristics of EBM parts may be controlled to produce tunable oxide thickness gradients. This behavior is important in designing post manufacturing machining and finishing processes, as these may be affected by the oxide thickness. The cohesion and adhesive strength of these surface oxides is inversely dependent on oxide thickness [44]. The oxide layer prevents corrosion while interacting with calcium ions [93,94].

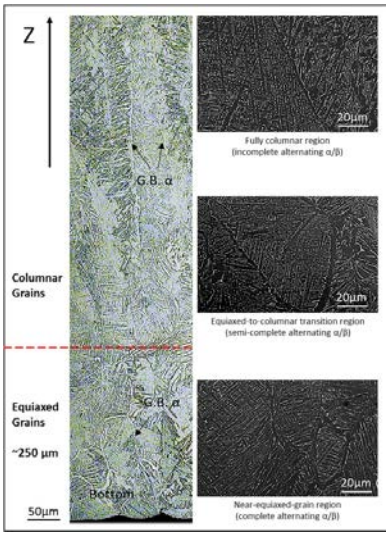

Figure 8 EBM fabrication of Ti-6Al-4V displays an equiaxed to columnar transition of β-grains through the initial 100 layers, with alternating α/β phase evolution as build height increases.

Reproduced with permission [89], 2015, Elsevier

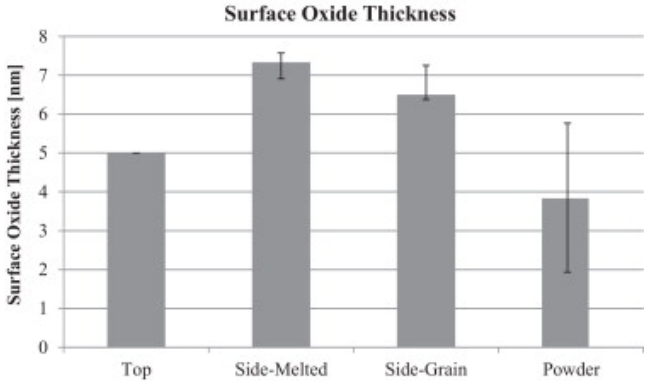

Figure 9 Surface oxide thickness relates to location (i.e. top or side) in EBM fabricated Ti-6Al-4V surfaces, and is related to variations in cooling rates.

Reproduced with permission [91], 2015, Elsevier

The porosity of parts produced by EBM is thought to occur largely as a side effect of the 'balling' phenomenon [24,95,96]. The formation of 'balls' is likely due to the simultaneous reduction in surface energy and surface area. This leads to the generation of small cavities, which is compounded by the effect of 'spattering', wherein the initial layers of the part have low resistance to electric repulsion occurring under electron beam radiation [96]. This effect is similar to that of 'powder blow-away' and results in the presence of large irregular pores. Pores may also arise from the presence of trapped argon during atomization. As mentioned previously, this porosity may be beneficial for bone-forming cells, but the difficulty in removing all entrapped powder is a limiting factor, as these particles are likely to contribute to wear and inflammatory responses.

As with SLM, parts produced by EBM are heavily influenced by process conditions and powder characteristics. Initial powder particle size is related to final density and surface roughness; parts fabricated with smaller sized particles, i.e. 25-45 μm (as opposed to the commonly used 45-105μm particle size range used for EBM), tend to have higher average peak to valley ratios and more un-melted particles attached on the uppermost surface [36,97,98]. Scanning velocity and line length have significant effects on heat concentration and material deposition. Increased scanning velocities and line lengths result in less heat provided to the area. Additionally, increased beam currents affect material deposition and ultimately may decrease the numbers of internal cavities/pores as well as larger agglomerates. This can be attributed to an increased driving force for sintering particles.

It is important to note that the effects of these parameters are interrelated. The ratio between beam current (and intensity) and scanning velocity is important in considering the final properties of the part [83,99]. Ideally, a low scanning velocity should be paired with a moderately high beam current to

produce a dense and flat part with pores at the outer layers [87]. The relation between powder size and surface roughness is notable and may be exploited to achieve specific topographies. Surface roughness provides an increased surface area and micro-texture, both of which are beneficial to cell adhesion.

The effects of varying porosity and surface roughness of EBM Ti-6Al-4V parts on *in vitro* and *in vivo* properties have been investigated by a number of groups, beginning perhaps most importantly with the work of Ponader et al. in 2008 [100]. Their experiment examined the behavior of human osteoblasts on EBM Ti-6Al-4V discs with a variety of surfaces (smooth, unpolished, hatched and sintered) over a period of 2 weeks. Higher cell viability and proliferation was observed on surfaces with R_a values of 0.077 µm, i.e. the smooth samples. As discussed previously, conflicting reports exist on whether roughness enhances or impedes osteoblastic proliferation and development, even on EBM Ti-6Al-4V surfaces. Ponader et al. in this study hypothesized that the key factor in the interaction between surface roughness and cell behavior was the propensity of the surface to allow cell to cell interactions. Cells prefer to attach in deep lying concave areas, i.e. between peaks/grooves (as this presents a low energy input configuration). Densely spread peaks (high R_q) and sharp peaks make cell-cell communication difficult, reducing the amount of cell proliferation – good cell proliferation was found in this study on surfaces with R_a values up to 24.9 µm and corresponding R_q values of up to 34.6 µm. Cell differentiation as indicated by the expression of various osteogenic genes/proteins such as ALP and osteocalcin (OC) was also examined – these markers were not significantly affected by surface roughness. It may be further hypothesized that surface roughness may affect only certain parts of the osseointegration process. In a follow-up study, Ponader et al. [86] investigated differences in the bone-regenerative ability of 60% porous vs. compact EBM Ti-6Al-4V cranial implants in a pig model over 60 days. While the porous implants displayed lower initial bone-implant contact (BIC) than the compact implants, a gradual increase in

BIC from almost 0 to 5% in the former was seen, as compared to a gradual decrease from approximately 30% to 9%. Thomsen et al. examined both as-produced and machined EBM Ti-6Al-4V femoral/tibial implants (compared with wrought Ti-6AL-4V implants) in a rabbit model and found between 29 and 41% BIC after 6 weeks [101]. Further *in vivo* work by Palmquist et al., in a sheep model investigating the long term biocompatibility of porous femoral and dorsal EBM Ti-6Al-4V implants compared to machined compact specimens showed BIC values of 57% after 26 weeks [102]. Puzzlingly, both compact and porous implants exhibited this level of BIC, despite the porous samples exhibiting pore sizes between 500 and 700 µm. BIC however appears to be a somewhat unreliable indicator of long term osseointegration, particularly in terms of extrapolation across models, and from animal models to human. Further work by Lv et al. [103] compared large and small pore sizes in scaffolds, and showed that the scaffold with smaller pore sizes, approximately 682±27 µm, showed greater MSC viability, reduced inflammatory cytokine release and increased ALP activity. This was assumed to be due to the higher surface area allowing for increased protein adsorption, leading to increased cell proliferation and differentiation. This reinforces the high BIC observed by Palmquist et al.[102] between porous implant and the host bone. However, it is insufficient to take two studies with different cell types as incontrovertible proof for the preference of bone-forming cells for smaller pores. Different pore sizes exhibit different pore architectures, especially as perceived by cells. Thus, both pore size and roughness are somewhat simplistic variables to manipulate in order to improve cell adhesion and proliferation – issues of topography (both nano and micro) and pore interior architecture are extremely important in determining cell behavior.

More detailed work on the potential irritation caused by EBM TI-6Al-4V parts was conducted by Haslauer et al. [104], who cultured human adipose derived stem cells on a variety of EBM produced discs (solid polished, solid unpolished, porous) and conventionally produced discs over a period of

7 days, with a particular focus on the comparative release of pro-inflammatory cytokines. The porous EBM discs showed the highest cell viability and proliferation, as well as the lowest release of pro-inflammatory cytokines (interleukin-6 and interleukin-8). Haslauer et al. concluded that average surface roughnesses of between 30 and 40 µm (corresponding roughly to the porous and solid unpolished specimens), as tested in this study, could provide an enhanced biological response in comparison to the roughness of classical sand-blasted and acid-etched implants, of between 3 and 4 µm. Meanwhile, Koptyug et al. [35] in their *in vitro* examinations of MG63 cells on EBM Ti-6AL-4V samples with a surface roughness range of between 14.7±4.2 µm and 22.2±5.9 µm (achieved by different etching times) determined there to be no significant differences in cell spreading or ALP activity with respect to surface roughness. Conflicting reports may be attributed to the use of multiple different cell types and vastly differing time scales of analysis.

2.3 DLD

The third AM technique that shows potential for biomedical applications is DLD. It differs from EBM and SLM in that it is a blown powder technique rather than having a bed. It combines material and energy delivery through the use of gravity powder feeding, allowing the stream to meet the energy source, creating a moving melt pool [74,105]. As with SLM and EBM, the energy source is used to fuse layers together to create either full parts or repair existing surfaces through cladding-like techniques [106]. Another key difference of DLD is the potential for using multiple powders within the same build. This allows for the production of bespoke alloys and compositionally graded parts, along with the usual range of complex and customized parts [107,108].

The primary components of DLD systems (Figure 10) include the following; a laser system, powder delivery systems (single or multiple powder hoppers), the controlled environment glove box, and

the motion control system (i.e. a Computerized Numerical Control (CNC) system) [107,109,110]. As with the previously discussed techniques, DLD production of parts begins with a design in STL format, which is sliced into 2D layers. This information is sent to the laser system and powder delivery nozzles, causing the assembly of each layer through the scanning of multiple tracks (in a user defined pattern). The presence of multiple powder hoppers and streams means that the composition of the deposited metal can be finely controlled; each hopper may be controlled individually to achieve the required composition [111–113].

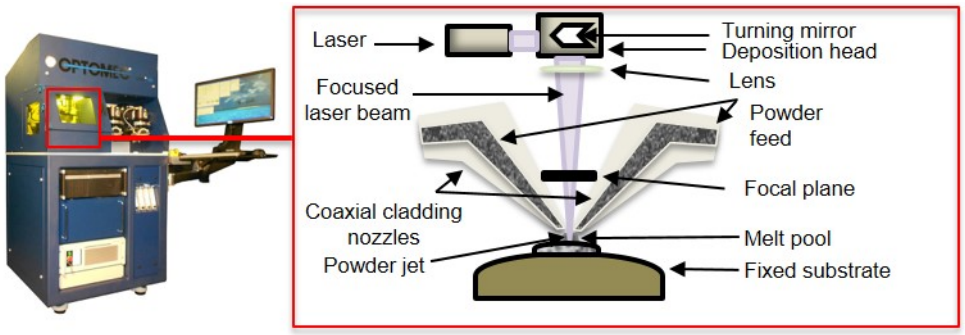

Figure 10 Schematic of DLD machinery showing powder streams converging at the point where they meet the focused laser beam, causing the formation of a melt pool on the fixed substrate, with a photo of a representative DLD machine.

The major variables in the DLD process are; laser/substrate relative velocity or scan speed (varies between 1-20 mm/s), laser scanning pattern, laser power (between 100 and 5000 W), laser beam diameter (usually maintained at 1 mm), powder feed rate (1-10 g/min), powder size range (10-100 µm in diameter, spherical particles required), and inter-layer idle time [114,115]. Each of these, and combinations thereof, greatly affect the final properties of any part produced. The cooling rate/thermal gradient ratio (R), and the temperature gradient at the solid-liquid interface (G) are particularly important, as the ratio of these two parameters affects solidification and therefore microstructure [105], as seen in Figure 11. Generally, equiaxed grain morphologies are produced by higher solidification rates, which are achieved by decreasing the ratio of G to R [105]. However, this

is not entirely indicative of final properties, which are also highly affected by part geometry and material properties.

DLD begins with the initiation of a melt pool, which is then superheated, and solidified. This involves complex powder-specific melt pool fluid mechanics and wetting behavior, as well as inconsistent boundary and inter-layer heat transfer [74,116]. Current DLD process optimization research concentrates on the modeling of these thermal gradients and stress-forming processes as a function of the process parameters [74,105,117]. Comprehensive reviews of the possibilities and properties of DLD fabricated parts have been completed and can be read elsewhere [115,118].

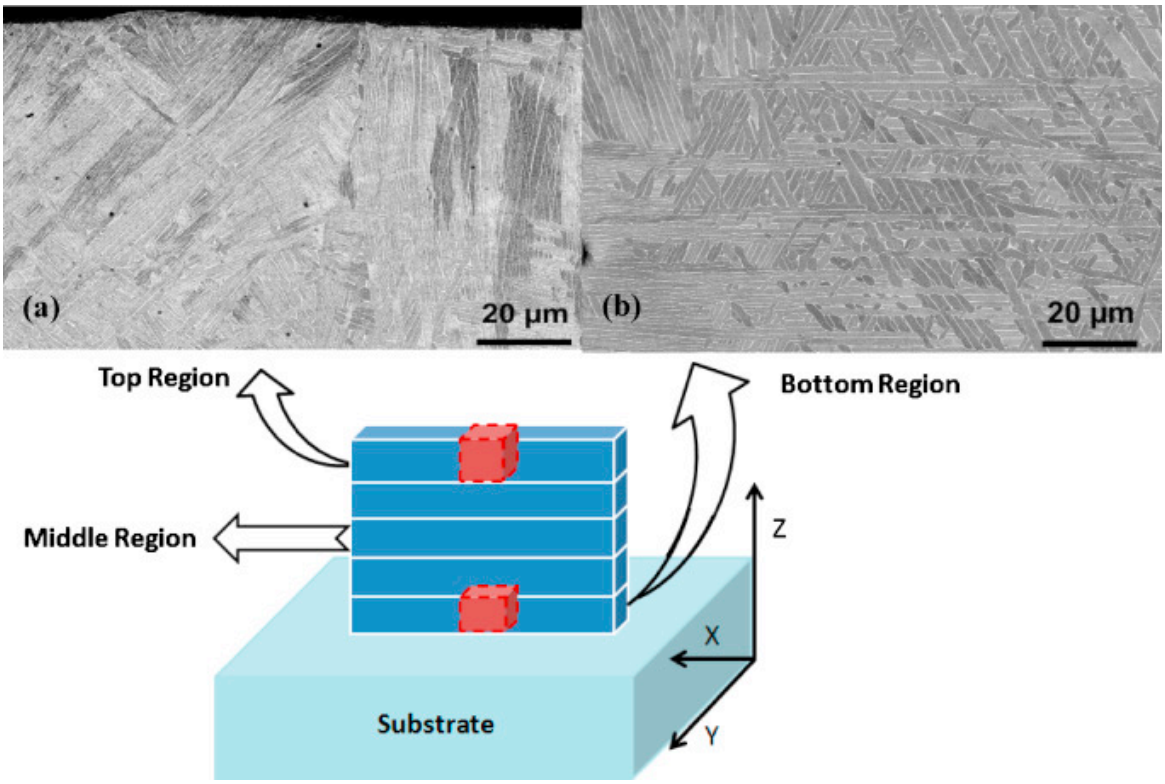

Figure 11 DLD part microstructure changes according to location within the part due to changes in thermal conductivity and repeated heating/cooling cycles, with a) showing the top region and b) showing the bottom region. While both regions display Widmänstatten structures, the top region shows colonies of fine lamellae and large laths, while the bottom region shows comparatively thicker lamellae.

Reproduced with permission [105], 2015, Elsevier

2.3.1 DLD part properties

Current issues with this fabrication technique can be broken down into three major categories – complex thermal history, anisotropy and build consolidation [119], with examples of the work done by various groups to elucidate these given in Table 2. As with the two previous processes, DLD fabrication results in parts with complex thermal histories due to the layer by layer nature of the process. As the melt pool generally penetrates multiple layers, multiple heating and cooling cycles occur, causing overlapping microstructural evolution processes and eventually non-homogeneous microstructures. Different overlapping cooling rates will form between layers, acting as another source of microstructural variation. Faster cooling causes the formation of discontinuous allotriomorphic α precipitates at existing β grain boundaries (Widmänstatten basket weave two-phase microstructures), while slower cooling rates cause the formation of continuous layers of allotriomorphic α precipitates, and coarser colony microstructures within grains [119]. Anisotropy results due to the preferential growth of columnar grains along the build direction, oriented with the 001 axis [119,120]. The width of these columnar grains are affected by scan speed (decreased width) and incident energy (increased width) [121]. The size of α and β laths has been found to increase with increases in laser power, feed rate and decreases in scan speed [121,122]. Texturing arises due to continuous re-melting of β grain tips upon themselves.

Finally, DLD part consolidation is typically incomplete due to significant porosity formed during fabrication (lack of fusion and internal pores). In studies of the interplay of processing conditions on part properties, multiple groups have found that porosity decreases with increased scan speed and laser power, and a high laser power combined with a low powder flow rate is required to reduce porosity [53,114,116,119]. Post-processing is a must for any part produced by DLD, and may include annealing to alter the volume fraction, size and aspect ratio of primary α laths, and HIPing, which closes planar pores and transforms martensite [123].

It has been reported that as fabricated DLD Ti-6Al-4V parts display higher tensile yield stresses than cast Ti-6Al-4V but brittle failure at low strains – 0.055 in the horizontal direction and 0.012 in the vertical direction [46]. Certain groups have produced DLD Ti-6Al-4V parts exhibiting average tensile strengths from 775 to 1270 MPa, similar to or greater than wrought Ti-6Al-4V [118,123,124]. The fatigue life of Ti-6Al-4V DLD components are generally lower than those of wrought parts due to process specific porosity and distinct microstructures.

Current research into clarifying the process dependent properties of DLD is focused on the characterization of thermal gradients, localized solidification phenomena and residual stresses, with respect to laser power and scan rate among other input parameters [115]. Very little work to date has examined the *in vitro* or *in vivo* performance of DLD produced Ti-6Al-4V parts, save for the work by Bandyopadhyay et al. examining the behavior of porous implants in a rat model over 16 weeks [125]. DLD produced implants of either 25.0% or 10.7% porosity were compared to implants with 2.8% porosity. Samples with 25% porosity displayed higher intra-pore calcium ion concentrations in comparison to all other samples. This was seen to peak at 6 weeks and decrease at 16 weeks, and was postulated to be due to ongoing bone remodeling processes causing inflow/outflow of other important factors. *In vitro* work using human-derived bone-forming cells such as human mesenchymal stem cells or human osteoblasts remains to be completed, as well as longer term *in vivo* work in alternate animal models.

2.4 Comparisons and commonalities of major techniques

Direct comparison of the three discussed techniques is difficult due to the range of processing conditions achievable for each. Process specific parameters such as scan rate, power supplied and

ultimate ED, as well as the interaction of these with material parameters such as powder size can lead to wildly different properties. However, some general comments can be made regarding the suitability of each technique for producing specific features.

SLM has a greater potential scan rate than comparable AM techniques such as EBM [50], and finer control with respect to scan rate and focus. SLM can be used to create parts with tailored porosities and hierarchical structures [71], or to deposit coatings onto ready-made parts. However, SLM has a lower energy efficiency than EBM – the laser beam can lose up to 95% of its energy due to reflection by metal particles within the build chamber [126]. Conflicting reports exist about the general surface roughness produced by EBM as opposed to SLM. The higher efficiency of EBM leads to a reduced amount of partially melted particles; however, this may depend on the build rate. In any case, EBM is generally reported to be the fastest technique, especially with respect to building fully dense Ti-6Al-4V parts [85]. The biocompatibility of parts produced by SLM and EBM was investigated by Wang et al. in dog, rabbit and guinea pig models [127], with cell attachment and spreading on the EBM and SLM samples shown in Figure 12. Multiple aspects of biocompatibility were examined, such as cytocompatibility, hemocompatibility and dermal irritation, with no significant differences being observed between parts produced by either technique over 2 weeks.

Parts produced through EBM generally have lower tensile strength and micro-hardness as compared with SLM due to differences in cooling rates[66]. In EBM, the chamber is maintained at temperatures between 650 and 700ºC, which, along with the aid of the vacuum, causes the relative cooling rate of the molten Ti alloy to be slower – SLM is carried out just above room temperature, and so the cooling rate is much more extreme.

It is well known that Ti-6Al-4V parts produced by AM techniques such as SLM, EBM and DLD display significantly shorter fatigue lives and fatigue strength than their wrought counterparts [128–132]. This presents a significant obstacle in the uptake of AM for use in the fabrication of orthopedic implants. This performance is particularly important given that during daily functional activities, peak bone loading occurs at relatively low frequencies (1-3 Hz), and for multiple cycles per day [48].

Differences in fatigue behavior arise due to process specific defects, the major contributors being lack of fusion pores, general porosity and the presence of majority α phases acting as sites for crack initiation [129]. Lack of fusion pores and general porosity in AM parts arise due to incomplete particle consolidation and/or the entrapment of gases during fabrication. Defects as small as 20 µm in size can contribute to fatigue failure, and AM process related defects can range up to 200 µm in size [128]. Larger and less spherical pores are more detrimental with respect to reduced fatigue performance. The fatigue strength of AM parts is heavily affected by the presence of micro-sized pores, while the growth of fatigue cracks is affected by residual stresses [52]. Two major failure modes are observed in AM parts; surface fatigue crack initiation and internal fatigue crack initiation [129]. Surface fatigue crack initiation occurs due to porosity and lack of fusion defects while internal fatigue crack initiation begins at α grain boundaries.

More widely, EBM parts generally display lower residual stresses immediately post fabrication due to the higher temperatures maintained within the build chamber during fabrication [129]. EBM produced parts can undergo phase decomposition during cooling within the chamber, leading to the formation of bimodal microstructures with fine α and β phases [128] which generally possess longer fatigue lives than majority α phase structures. SLM parts generally display inferior fatigue performance than both EBM and LENS produced parts due to higher residual stresses [98]. Meanwhile, LENS parts have been shown to have better lower cycle fatigue performance but poorer higher cycle fatigue performance than mill annealed samples [133]. However, fatigue performance

comparable with wrought and annealed Ti-6Al-4V has been achieved in AM parts, with the use of post-processing treatments such as heat and HIP treatments. Heat treatments serve to reduce the amount of residual stress within the parts, while HIPing consolidates parts and reduces the amount of internal defects. These in addition with the size reduction of α phase clusters are potent mechanisms for reducing the initiation of internal fatigue cracks [129].

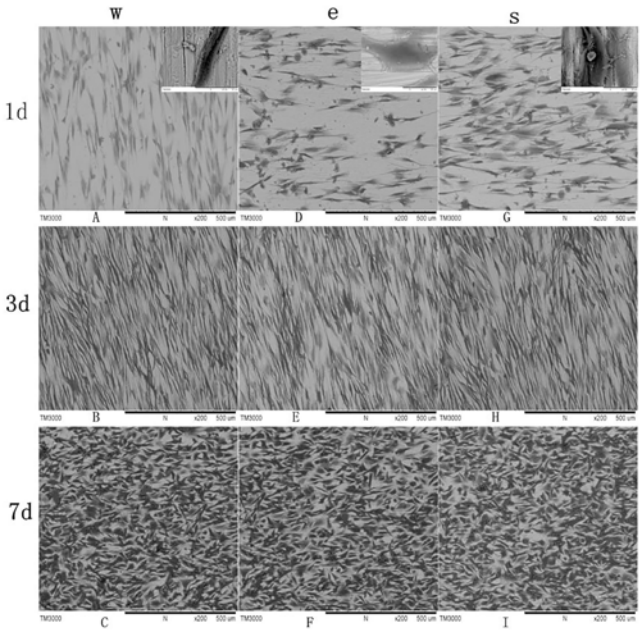

Figure 12 Mesenchymal stem cell seeding on wrought (w), EBM (e) and SLM (s) Ti-6Al-4V samples showing that cell attachment and spreading at all time points was comparable on the EBM and SLM surfaces to the wrought Ti-6Al-4V surfaces (indicating good biocompatibility)

Reproduced with permission [134], 2016, PLOS ONE

In comparison to other AM processes, DLD allows for simultaneous deposition and part forming due to the union of the material and energy source in the same region. Compared to SLM or EBM parts, DLD components display higher surface roughnesses immediately following fabrication, and require post-processing to reduce the microstructural inhomogeneities accumulated during fabrication. However, DLD has the potential to produce parts with compositional differences, due to the multi-nozzle capabilities. This is of interest for orthopedic implants, as compositions may be

varied to produce functional variations across parts, corresponding to different requirements across a part, for example in fracture plates.

3. Pre-print considerations

3.1 Material design

Currently, 70-80% of orthopedic implants are fabricated from Ti alloys, such as Ti-6Al-4V [135]. However, certain alloying elements have been reported to cause harmful effects when leaching out of the implant - vanadium is linked to heavy metal toxicity, while Al has been linked to the increased likelihood of developing Alzheimer's disease [136]. The current focus is towards alloys with bio-active elements which have greater osteo-inductive properties, as well as mechanical properties closer to that of bone. These alloys, when used in conjunction with AM techniques, may facilitate significant improvements in initial implant fixation and bone healing. Ultimately, the role of an orthopedic implant is to work in tandem with host bone to produce a combined structure which can both withstand normal physiological loads and minimize local stress shielding. To this end, alloying elements such as Nb, Ta, Zr, and strontium (Sr) are being widely investigated. These are β stabilizing elements with low modulus, high strength and high resistance to corrosion [9]. Additionally, Zr acts as a neutral element facilitating the formation of homogeneous solid solutions in α/β phases [137].

Low modulus β phase Ti alloys are being developed worldwide [138–141]. The β phase of Ti has a body centered cubic structure with high symmetry (as compared to the hexagonal close packing of α Ti) – this is responsible for the reduced modulus and increased wear resistance in comparison to α-rich titanium alloys [142,143]. Investigations have been conducted into the effects of differing ratios of β-stabilizing alloying elements such as Nb, Zr and Ta through AM fabrication) [19,144] However, there is controversy over the ideal alloy composition – the amount of each element must be

balanced to ensure that the AM fabrication is possible, while minimizing costs and improving performance beyond that of conventional alloy compositions and/or conventionally fabricated parts.

The current focus is towards Ti-Nb-Zr-Ta and Ti-Nb-Ta-Zr compositions, with Ti-35Nb-7Zr-5Ta and Ti-29Nb-13Ta-4.6Zr showing the most promise, with modulus values of ~55 GPa (20% lower than comparable alloys) [22]. These alloys have moduli in the range of 40-80 GPa, which, when compared with the modulus range of cortical bone of 10-30 GPa, presents a significant improvement in modulus matching[3,19,135,144,145].

While these alternate alloys have significant potential benefits, it must also be noted that their use in AM processes is currently limited due to issues with powder formation. The majority of currently available pre-alloyed powders are of structural steels and alloys with long research histories. DLD is therefore the leading technique in the investigation of new generation β phase Ti-based alloys. DLD allows for the in situ formation of multiple alloy blends through changing the powder feed rates from various hoppers containing Nb, Zr, Ta and similar powder feedstocks. Banerjee et al. have pioneered the use of combinatorial approaches to the development of β phase Ti alloys for orthopedic implants through the use of DLD [110].

3.2 Raw materials

The single most important aspect of AM, particularly powder bed fusion methods such as SLM and EBM is powder morphology and size. Successful powder bed fusion requires high flowability powders composed of regular, spherical particles within a tight size range. [60,146]. SLM requires particles in the diameter size range of 10-45 µm, while EBM requires slightly coarser particles in the size range of 45-105 µm.

Powder flowability is a result of the following powder properties; density, compressibility, cohesive strength, electrostatic forces, surface tension and space filling characteristics [44]. Powders with excessively fine particle size distributions will experience high rates of electrostatic repulsion [60]. This will adversely affect flowability, as the static forces will cause rolling and recoating to occur unevenly. However, a larger average particle size reduces the driving force for sintering [27]. It is therefore important that the particle size distribution of the powder remains within a tight threshold. Particle shape is also important, as it relates to the efficacy of particle packing. This affects the efficiency of layer forming and therefore final part properties. Flowability is linked to shape factor, i.e. the shape of the particles independent of dimensions - here, the most important shape factor is sphericity.

It is important to note that the size and shape of the powders used are contingent on the methods used to manufacturing. The major powder forming methods are gas atomization (GA), plasma atomization (PA) and the plasma rotating electrode process (PREP), as well as induction plasma melting. GA has been reported to produce particles with a larger mean size, while PREP produces more spherical particles [53,147–149]. Another method for forming powders with spherical morphologies is the induction plasma melting method. Smaller relative powder sizes generally lead to better surface resolution and appearance [32]. A visual comparison between fabrication types and the powder morphologies before and after printing is seen in Figure 13.

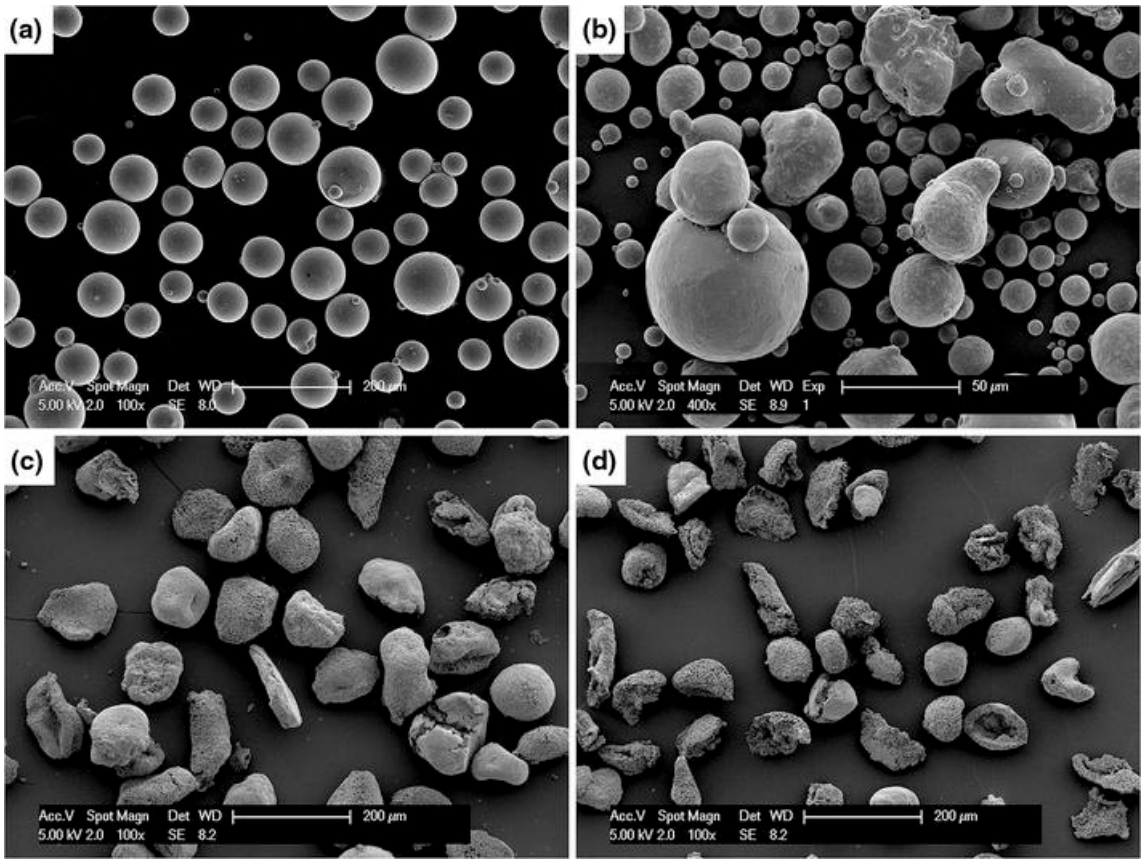

Figure 13 SEM images of a) virgin, b) used Arcam Ti-6Al-4V 45–106 µm powder (undocumented but <30 times), c) 75–106 µm and d) 45–75 µm as-received novel Ti precursor. Different processing and preparation techniques are thus shown to produce vastly different qualities of powder, and thus the choice of feedstock for powder-based AM techniques is of extreme importance.

Reproduced with permission [148], 2015, The Minerals, Metals and Materials Society

Though size and shape are important, the characteristics of the specific AM process must also be considered. SLM produced parts have better qualities when produced with a unimodal fine particle size distribution, while EBM produced parts have better qualities when the initial powder has a bimodal size distribution [44]. This allows better packing through improved layer filling and densification.

Notably, powders used during fabrication of parts using powder bed fusion methods may be recovered and reused. However, the characteristics of these recovered powders are often quite different to their initial properties. Powder recovery usually occurs through high pressure air blasting, vibratory processing or a combination thereof [44]. The work of Tang et al. revealed that the more times Ti-6Al-4V is used in EBM, several important properties change; average particle size decreases and particle size distribution becomes narrower resulting in improved flowability, oxygen content increases due to air exposure and humidity (however this does not occur in the presence of helium), Al and V content decrease slightly due to vaporization in vacuum, and particle sphericity decreases [150]. Additionally, the amount of satellite particles and agglomerates decrease due to repeated sieving between fabrication cycles. Therefore Tang et al. recommend not to re-use powders more than 4 times without the addition of virgin powder, and powders should not be reused more than 16 times due to the significant amount of particle distortion and surface roughness [150]. This detail, i.e. the number of times the powder has been recovered prior to sample fabrication, is rarely reported in articles examining metallic AM processes. Going forward this is an important parameter to consider and report, especially given the effect of powder morphology on part microstructure and properties.

3.3 Part design and support structures

Part design for Ti-based orthopedic implants can be roughly split into two categories – dense implants with surface features, and cellular scaffolds or solids (open forms, unit cells, functionally graded structures) [85]. Surface features such as additional holes for bone screws or the addition of small surface bumps can easily be added into CAD files through programs such as **Solidworks (Dassault Systemes), Mimics (Materialise)** and **Rhino (Robert McNeel & Associates)**, or freely available and online programs such as those available from **Autodesk** or **Sketchup (Trimble Incorporated)** [42,43]. Cellular scaffolds with interconnected pores (Figure 14) offer a range of

benefits in comparison to traditional dense structures, the most important of which are; the potential to reduce stress shielding through closer property matching to bone, and the facilitation of bone cell ingrowth [85,151]. Pore shape, amount and porosity gradients can be altered in the design stage to produce parts with specific stiffnesses and strengths (as porosity increases, stiffness and strength generally decrease) [85]. The minimum pore size for cellular scaffolds which can allow bone in-growth has been stated as 50 µm, however in terms of practical application, pore sizes of 300µm are recommended – this ensures that cell proliferation and penetration can continue (no one pore should be occluded by a cell), and also ensures permeability and flow of nutrients/wastes [85,152,153]. Larger pore sizes are also more conducive to 3D printing processes, particularly in the depowdering stage. Graded scaffold structures are the most promising designs in terms of improving osseointegration, as these have the potential to closely mimic the complex structures found in bone[81]. The literature contains a wealth of studies examining novel hip and knee designs with superior osseointegrative abilities. Notably Melancon et al present morphological and mechanical property maps for SLM Ti-6Al-4V, emphasizing the ability to tune stiffness to native bone while accommodating for manufacturing discrepancies. Arabnejad et al present a high strength, porous implant model with a 75% reduction in modulus mismatch in comparison to solid models [154]. The testing, success and uptake of these various alternative implant designs depends on first achieving a complete understanding of the characteristics of each AM process, and the properties of parts produced by each process.

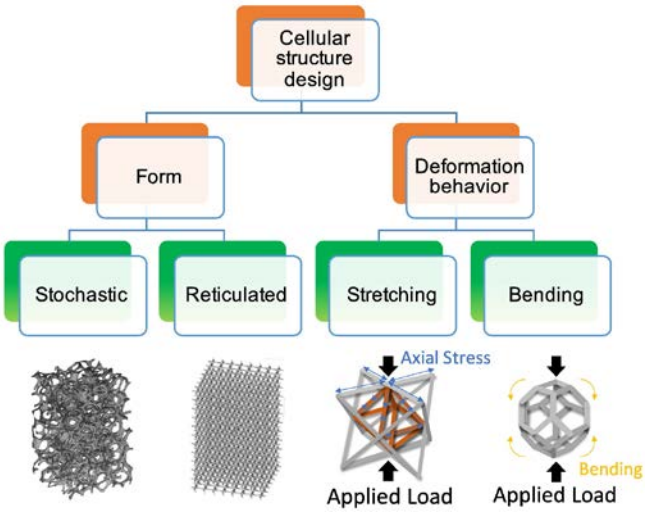

Figure 14 Map of possible cellular scaffold types in terms of form and deformation behavior.

Reproduced with permission [85], 2017, Elsevier

The practical capabilities of EBM and SLM are informed by the complexity of the design. Any surface at a <45° to the previous layer will require a support structure [155,156]. These structures act as anchors to the build plate, prevent part warpage due to residual stresses, and aid in heat conduction away from the part. As mentioned previously, software such as Magics (Materialise) or Simplify3D (Simplify3D) may be used to automate or customize the design of support structures such that they are easily removed from the final part, however, the surface to which the supports were attached will generally show higher surface roughness than the rest of the part, in the micrometer range [157–159]. Support structures are typically built to resemble trusses, but can take many other forms, for example blocks, points or lines (Figure 15) [156,157]. The incorporation of teeth into the part of the support contacting the part can aid in removal – the spacing between teeth, the height of the teeth and tooth contact area can all be altered according to the specific requirements. However, often even the presence of support structures may be insufficient to prevent warping or to prevent the part from peeling off the plate due to excessively high residual stresses, particularly in Ti-based alloys. In such extreme cases, a part redesign may be necessary. Other strategies to reduce the amount of

support structures required include rotating the build orientation, as well as using algorithmic methods in the design phase. Various researchers have proposed algorithms for optimizing the amount and location of support structures, for example the methods suggested by Frank [160] and more recently Strano [158], however the use of Taguchi methods show the most promise [155]. There is currently a gap in the literature regarding the proper design and application of support structures specifically for Ti-based orthopedic implants with respect to the extremely high amounts of residual stresses formed. Going forward, this will be extremely important in the manufacture of delicate parts such as customized fracture plates and screws.

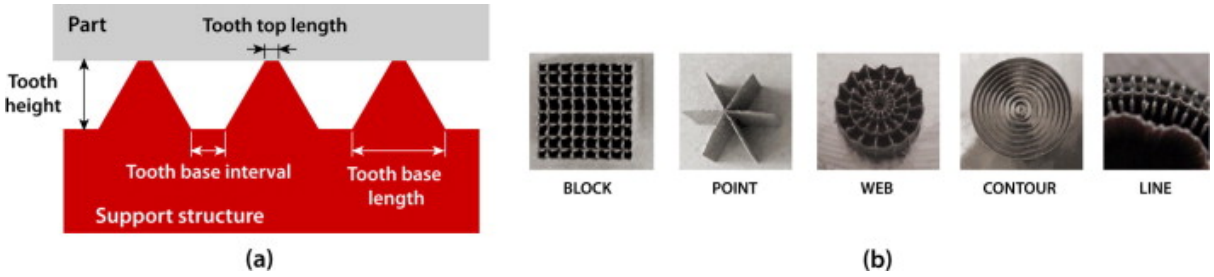

Figure 15 Examples of different types of support structures used for SLM and EBM parts with a) showing tooth characteristics and b) showing alternative support structure designs.

Reproduced with permission [155], 2014, Elsevier

4. Post-processing considerations

4.1 Heat treatments

SLM and EBM parts are both notable for the formation of non-equilibrium phases due to the rapid heating/cooling cycles produced during fabrication. This causes a build-up of thermal stresses and segregation phenomena. Heat treatments may be applied to partially alleviate the presence of these stresses [161]. Vrancken et al. studied the effects of heat treatments on SLM produced Ti-6Al-4V parts, and reported the conversion of α' phase to a lamellar mixture of α and β phases [110]. The samples were heated to above 995 ºC, where large β grains formed. These decomposed into lamellar α and β phases on cooling. A post-treatment at 850 ºC for 2 hours followed by furnace cooling increased ductility to ~12% compared to 7% [161]. Transformation from columnar to

spherical β grains has also been observed through the application of heat treatments above 1000ºC [162]. The presence of β grains has been observed at treatment temperatures as low as 700ºC, however, overall martensitic morphology appears to be dominant until larger α plates form at higher temperatures [75]. An instructive comparison between the various microstructures produced by heat treatments can be seen in Figure 16.

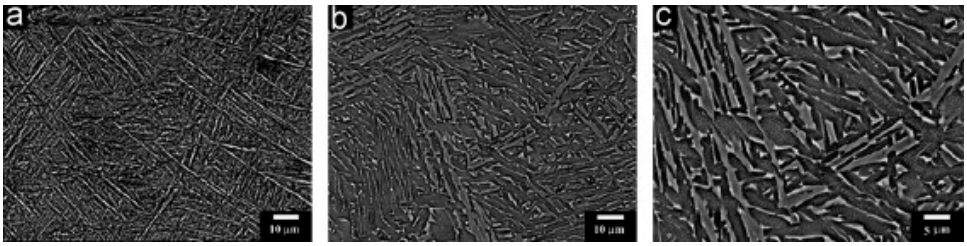

Figure 16 Microstructural changes can be observed according to the different post-processing heat treatment conditions of SLM Ti-6Al-4V, a) shows an SLM sample annealed at 600ºC, b) shows an SLM sample annealed at 700ºC, with α plate formation, and c) shows a HIPed SLM sample.

Reproduced with permission [75], 2013, Elsevier

4.2 Surface patterning

The ultimate goal for the surface modification of permanent Ti implant surfaces (i.e. those required to osseointegrate) is to improve osteoblast adhesion and differentiation, leading to increased bone deposition. *In vivo*, osteoblasts work within nano-scale topographies, with collagen fibrils and HA having lengths of 50 to 300 nm and widths of ~0.5 nm respectively [15]. Thus, osseointegration is known to be affected by surface roughness and porosity [15], although little agreement exists in the literature on the specifics, be it the 'optimum' pore size range, porosity percentage, or the average roughness.

Osteoblast or osteoblast-like cells grown on roughened Ti surfaces (ideal pore sizes of between 100 and 500 μm, with ideal porosity of ~60%) have been shown by some groups to present reduced

proliferation, enhanced differentiation and the up-regulation of genes related to bone deposition [15,163,164]. Conversely, other groups indicate that osteoblast proliferation is improved on smooth surfaces with Ra values of less than 0.5 µm [165–167]. Numerous mechanisms are thought to be in play, with surface roughness dictating protein absorption and subsequent intracellular signaling cascades, particularly those related to integrins and fibronectin [168]. Higher pore volume has been shown to be roughly correlated with higher Ca+ concentration within pores [125], facilitating osteoblast adhesion and osteogenic cell ingrowth. Further into the osseointegration process, micro-rough surfaces have been shown to reduce osteoclast activity, thereby decreasing the resorption of bone. Thus, the role of roughness in osseointegration can be thought of as important to the remodeling process, or rather the balance of activity between bone forming and bone resorbing cells, with surface roughness affecting multiple processes at different time scales.

Current methods used for surface texturing of Ti-based implants can generate features on the micrometric or nano scales, through physical, chemical, electrochemical deposition and biochemical methods [169], however a major consideration in the application of surface texturing is the effect on the fatigue and other mechanical properties of the part. Line of sight methods such as plasma spray coating are falling out of favor due to their inability to treat complex geometries. Biomimetic methods such as anodization and acid etching are most commonly used to roughen AM produced Ti-6Al-4V implant surfaces [170].

4.3 Coatings

4.3.1 Calcium phosphate-based coatings

Coatings are also of great use in facilitating osteoblast interactions with (cement-less) implant surfaces, and are an important post-processing modification to consider in the development of AM implants. Calcium phosphate or hydroxyapatite (HA) containing coatings have long been shown to

improve future bone deposition and osseointegration through ion-exchange facilitated protein deposition [171,172]. Multiple methods for hydroxyapatite coating deposition have been investigated including plasma spraying and chemical vapor deposition, and newer biomimetic solution-based precipitation methods. As far back as 1993, Søballe et al. were able to show that plasma sprayed hydroxyapatite coatings on Ti-based implants improved bone ingrowth into implant surfaces, even in cases of osteopenic host bone stock (shown in a canine model) [173]. Eckardt et al. were also able to show an improvement in bone contact (65% HA-coated implant vs. 14.7% uncoated implant) with the use of HA-coatings on implants in dog models, over a longer observation period of 2 years [174]. The application of these coatings to AM implants is a potent strategy for improving fixation.

4.3.2 Refractory ion containing coatings

Coatings containing bio-active molecules or elements can also be used to act as stimulation for bone forming processes. Chief among the bio-active elements currently under investigation for their abilities to improve bone bonding are the refractory elements Ta, Nb, Zr and Sr.

Tantalum bonds well to bone and forms an apatite-like layer in simulated bodily fluid, and is noted for having high fatigue and corrosion resistance [175,176]. The 3D geometry of porous Ta is similar to that of trabecular bone [177]. It also has a high surface energy and wettability, increasing the likelihood of effective cell attachment and distribution [178]. Numerous studies have shown increased bone-forming behavior on Ta containing surfaces as opposed to plain Ti surfaces [177–180]. Balla et al. demonstrated the use of DLD to deposit a Ta coating on Ti, with significantly higher cell density on Ta coated Ti at all time points. After 14 days of culture, a 6-fold increase was observed on Ta coated Ti as opposed to uncoated Ti, accompanied by increased filipodial extension by cells [178]. Tantalum however has a high cost of manufacture, making it suitable only as a minor alloying element. It has a low laser absorption coefficient due to low electrical resistivity. This has a large

effect in SLM, where the shallow thermal gradient within layers will affect the melt pool characteristics and therefore the microstructure of the part.

Niobium has also has seen use in bioactive coatings and alloys [8,71,135,181]. Elemental Nb also displays good wear resistance and biocompatibility. The presence of Nb has been seen to improve cell attachment and growth, and has a beneficial effect on cell morphology, with adhering cells displaying multiple extensions and spreading [71]. Zhang et al. fabricated porous Nb coating on Ti substrates using SLM [71]. This coating, composed of Nb_2O_5 and NbO_2, displayed a pore size of 15-50 µm, with an average hardness of ~392 HV. This relatively short-term study showed that Nb coated Ti showed significantly higher numbers of cells after 11 days, indicating a potential enhancement of proliferation. Zhang et al. also noted the lower melting temperature of Nb as opposed to Ta (2468ºC vs. 3017ºC). However, it is also quite expensive and has a low laser absorption coefficient. It has not either, to date, seen wide uptake in coating applications, being used more frequently as an alloying element.

Perhaps the most promising element for use in orthopedic implants is Sr. The presence of Sr ions as substitutions in HA layers has been shown to enhance bone formation and inhibit bone resorption [15]. Sr is an alkaline earth metal with properties like that of calcium. For this reason, it functions similarly to Ca in the body. Strontium acts on bone cells to control bone resorption and regulate genes involved in osteoblastic cell replication, differentiation and survival. More specifically, it inhibits osteoclasts and therefore bone resorption, and improves the differentiation and activity of osteoblasts [182–188]. Li et al. investigated the effects of 10% Sr substituted HA coatings on implant fixation in a rat model, and found that after 12 weeks, bone to implant contact increased by 49.9% as compared to implants coated with non-substituted HA [189]. Subsequently Yang et al. investigated

the effect on bone marrow mesenchymal stem cell osteogenesis of coating Ti with Sr substituted nano-hydroxyapatite deposited via electrochemical techniques. Sr substitution significantly enhanced ALP activity in bone marrow stromal cells (BMSCs) in comparison to non-substituted HA coatings [190].

4.4 Surface finishing and sterilization

All AM processes produce parts with relatively high surface roughnesses (>Ra 15 µm), which relates to the presence of semi-melted particles left on outer surfaces following fabrication. As discussed previously, these areas experience different cooling rates due to heat transfer from the melted part directly to the powder bed, and do not undergo re-melting cycles from subsequent layer laser penetration. This roughness has important consequences with respect to both material performance and biological responses (e.g. inflammation, osseointegration), and combined with the high notch sensitivity of Ti-6Al-4V mean that as-fabricated AM parts will generally exhibit shorter fatigue lives. Without surface finishing, semi-melted particles on AM Ti-6Al-4V surfaces have the potential to detach following implantation, and cause localized osteolysis [191]. Semi-melted particles have been shown to affect cell migration and reduce the effective surface area for integration [191,192]. However there is little data in the literature at present to quantify this with regards to specific processes and parameters used. Of the few studies currently published, Vaithilingam et al and Matsoukova et al performed in-vitro studies to investigate the potential cytotoxicity of particles detaching from the surface of AM Ti-6Al-4V implants and found no evidence of particles detaching even without post-processing [191,193].

In any case, the surface finish of AM parts is of paramount importance in post-implantation osseointegration. Common methods for improving the surface finish of AM parts include

mechanical blasting, chemical etching, laser ablation, micromachining, vibratory grinding and polishing [194]. These processes are generally line-of-sight dependent, and so difficulties arise in the appropriate finishing of intricate internal structures such as pores and lattices. Relatively few studies have compared processes but initial evidence suggests that sand blasting and electropolishing are inappropriate as the finishing media can be difficult to remove. Specifically, sand blasted parts display surfaces with impregnated blast media in the form of AlO_x elements – Al ions in the outer oxide layer of Ti-6Al-4V have been shown to reduce the oxide stability and increase the likelihood of Al ion dissolution [191,192]. Electropolishing and chemical etching can lead to the formation of micropits, increasing oxygen infiltration, as well as destabilize the native oxide layer, reducing corrosion resistance [191,195]. Conversely, Longhitano et al investigated the combination of various finishing processes on SLM Ti-6Al-4V, and found that blasting followed by chemical etching produced parts with and R_a of approximately 4 µm – this can be explained by the stepwise action of blasting removing material from the surface, and subsequent etching removing blast media from the surface.

Surface finishing techniques such as laser ablation and milling show more promise. Mohammad et al investigated the use of laser ablation in reducing the surface roughness of EBM Ti-6Al-4V and were able to achieve a surface finish of 13 µm (R_a) with a laser fluence of 150 J/cm^2 [196]. Bagehorn et al, compared various finishing techniques on SLM Ti-6Al-4V and found milling to produce the smoothest surface compared to blasting, vibratory grinding and micro-machining [130]. Additionally, milling improved the fatigue performance of the SLM Ti-6Al-4V to replicate that of forged Ti-6Al-4V.

It is important to note that surface finishing processes are ‘line of sight’ limited, and so intricate internal structures like pores or lattices are difficult to finish, much less inspect. In the same manner

as finishing processes are ‘line of sight’ limited, so too are sterilization methods. Commonly used sterilization processes for orthopedic implants, including AM, extend to ethylene oxide gas sterilization (exposure to ethylene oxide under vacuum), steam sterilization (exposure to high temperature steam) and γ radiation. Of these, γ radiation is the most favorable, as it has the potential to sterilize both intricate internal structures, internal voids (defects) and complex geometries without leaving behind sterilization products [197]. To our knowledge, no studies have examined the effects of sterilization on the mechanical properties of AM parts, and this remains a significant gap in the literature.

At present, the assessment of the efficacy of finishing and sterilization processes occurs on a case by case basis. As the technology develops, so too do regulatory concerns and guidelines, and at present the Food and Drug Administration of the United States of America requires premarket submissions for medical devices in 3D printing to provide validation of any cleaning and sterilization process used [198]. The relevant regulations and guidelines are discussed further in Section 6.

5. Case studies

Table 2. Selected AM processing parameters and properties of Ti-6Al-4V parts

Process	Process parameters						Properties								Ref
	Particle size (µm)	Layer thickness (µm)	Scan rate (mm/s)	Laser power (W)	Spot size (µm)	Hatch spacing (µm)	Young's modulus (GPa)	Yield strength (MPa)	Ultimate tensile strength (MPa)	Elongation (%)	Vickers hardness	Density/ porosity	Surface roughness	Other	
SLM	15-70 (PA*)	50	225	157	70	100	xz; 115±6 zx;119±7 xy; 113±5	xz; 978±5 zx; 967±10 xy; 1075±25	xz; 1143±6 zx; 2228±3 xy; 1199±49	xz; 118±0.5 zx; 8.9±0.4 xy; 7.6±0.5	-	-	upskin – 6.834 sideskin – 28.587 (Ra in µm)		[199]
	15-75 (PA*)	50	58	42	30	30	119±7	-	-	-	500	99.4±0.2%	-		[200]
	5-50 (PA*)	30	1600	250	52	60	109±7	967±10	1117±3	8.9±0.4	-	-	-		[161]
	30 (GA**)	50	200	200	130	50	-	910±9.9	1035±29.0	3.3±0.76	-	-	-		[98]
	15-25 (GA**)	30 60 90	686 710 102	175 375	-	12 18	-	1100	-	-	-	-	-		[201]
	20-50 (GA**)	20	800-1500	150-200	150	75	-	>1 (0.2% proof stress)	1200	<10	-	0.1%	-		
	43 (GA**)	30	710	175	-	150	-	-	-	-	-	-	-		[51]
	40	30	450	100	-	-	-	1008±30	1080±30	1.6±2%	-	-	-	mean fatigue life of 27,000 cycles	[52]
EBM	30 (GA**)	build parameters absent						1150 1100	1200 1150	25% 16%	3.6 3.8 3.6 4.1			for EBM1 (top end) for EBM2	

Process	Process parameters						Properties								Ref
	Particle size (µm)	**Layer thickness (µm)**	**Scan rate (mm/s)**	**Laser power (W)**	**Spot size (µm)**	**Hatch spacing (µm)**	**Young's modulus (GPa)**	**Yield strength (MPa)**	**Ultimate tensile strength (MPa)**	**Elongation (%)**	**Vickers hardness**	**Density/ porosity**	**Surface roughness**	**Other**	
														(top end)	
								1170	1230	12%	380			for wrought Ti64	
	Table d45-100 (GA**)	70	Arcam standard	60 kV	Arcam standard	Arcam standard	180±15				425±50				[36]
	45-100 (GA**)	100	energy input per unit length = 0.55 J/mm, line offset of 1.0 mm				parallel loading = 12.9±0.9 perpendicular loading = 3.9±2.1 complete infiltration of osseous tissue	parallel loading =148.4±3.5 perpendicular loading =127.1±29.2				mean pore size = 0.45 mm porosity = 61.3%		designed porosity	[86]
	45-105	50	arcam standard	arcam standard	arcam standard	arcam standard		top layer =823.4±0.1 bottom layer =851.8±5.8	top layer =940.5±6.5 bottom layer =964.5±0.3	top layer =13.2±0.7 bottom layer =16.3±0.8	top layer =319±5, bottom layer =327±5	-	-		[89]
	45-105	50						10 mm 1; 851.8±5.8 10 mm 2; 836.6±8.7 10 mm 3; 827.9±0.9 10 mm 4; 823.4±0.1	10 mm 1; 964.5±0.3 10 mm 2; 953.7±4.3 10 mm 3; 944.5±5.8 10 mm 4; 940.5±6.5	10 mm 1; 16.3±0.8 10 mm 2; 15.2±1.2 10 mm 3; 14.0±0.5 10 mm 4; 13.2±0.7					
DLD	50-150	-	22.5 mm/s	200 W	-	-						30%			[108]
	150 mesh	-	635 mm/min	350 W	-	hatch distance of 0.38 mm, with layer spacing of 0.25 mm								single β phase formed, average grain size of 50 µm	[202]

Process	Process parameters						Properties								Ref
	Particle size (µm)	**Layer thickness (µm)**	**Scan rate (mm/s)**	**Laser power (W)**	**Spot size (µm)**	**Hatch spacing (µm)**	**Young's modulus (GPa)**	**Yield strength (MPa)**	**Ultimate tensile strength (MPa)**	**Elongation (%)**	**Vickers hardness**	**Density/ porosity**	**Surface roughness**	**Other**	
	45	30	1250	170	100	-	-	1185	1293	6.23	402.81±11.31	-	35±5	-	[119]
	15-45	50	EOS default	EOS default	100	-	114.9	1093	1130	-	-	95-99% dense	11-13	-	[46]
	(GA**)	30	0.6 m/min, powder feed rate = 1 g/min	330	-	50	-	1005	1073	4	-	-	-		[133]
	89 (PREP†)		10.6	2 kW	-	-	111±3	938±22	1048±23	23±3					

6. A clinical perspective

The bulk of research into the properties of AM fabricated Ti-based parts has been from a metallurgical or biological perspective, using part geometries far removed from actual implant designs. With this research in its infancy, relatively little long-term clinical data is available, and so actual bench-to-bedside feasibility is poorly understood. With the advent of AM, and the increasing practicalities of producing tailored structures, it is important to consider how this new technique will be received by clinicians and their patients, particularly with regards to such aspects as financial viability and quality control/regulation. From the perspective of an orthopedic clinician, AM technologies offer three major advantages in comparison to conventional manufacturing; the ability to create Patient Specific Implants (PSIs) by combining 3D Digital Imaging and Communications in Medicine (DICOMs) with standard implant designs, utilize these in surgical planning, and to produce aids for surgical education [42,45,60,203–205].

PSIs in orthopedics have historically been created only for patients with rare diseases or complex reconstructive needs, i.e. approximately 1% of all implanted devices [39]. However, computational power and technology has improved significantly in the past 10 years, allowing more widespread uptake of AM for PSIs, particularly for patients with bone deficits as follows [206,207];

- Trauma in the form of extreme fractures arising from long term osteoporosis – implants can be designed to include ‘fixation features’ such as extra holes for bone screws.
- Bone cancers, which accounted for 0.2% of new cancers in the U.S. in 2014, 26.9% of which arose in patients younger than 20 years old – standard designs can be adapted to both include ‘fixation features’, as above, or to compensate for areas of bone loss local to the implant.

- Congenital or developmental deformities such as spondyloses or scoliosis – implants can be made with reference to DICOMS to directly complement the non-standard structure of the patients' bone in establishing optimal performance.
- Osteoarthritis and other degenerative joint diseases which are expected to affect 25% of adults in the U.S. by 2030 - custom shaping allows for optimized bone preservation.
- Bone infection or decay, for example through osteomyelitis or dental caries – DICOMS and 'fixation features' can be combined to produce implants that support natural function.

Atypical bone anatomy, poor bone stock and extreme iatrogenic bone loss are cases where AM can provide great value. Many patients requiring orthopedic implants will present with poor bone stock due to conditions such as osteoporosis, as well as long term steroid treatment [173]. These patients will have significantly lower bone turnover and remodeling activity, and thus there is a significant need in this sector for 'smarter' implant behavior [2]. These pre-existing conditions contraindicate the use of standard implants, as these are likely to both fit poorly and create additional problems in the months and years following implantation due to poor fixation (loosening, wear debris formation) [10,168,208].

In this regard, AM has the potential to improve on classical orthopedic implant designs, which have to date been limited by conventional manufacturing techniques. Direct patient data (DICOMs) can be used to make exact copies of removed bone sections or to guide the design process in terms of inserting additional features likely to improve fixation [209]. Potential features to reduce stress shielding include; unique internal structures, latticing to maintain strength but not stiffness, surface texture, and graded porosity [210]. The design of reservoirs with pharmaceutical payloads (slow or fast release therapeutics, e.g. chemotherapeutic agents, bone growth promoters or antibiotics) is a popular new area [206,211]. Thirdly, AM fabrication lends itself well to producing low volumes of

highly complex parts – this means that pediatric implants can be sized specifically and iteratively for growing pre-pubescent patients, and take into account the complexities of young and incompletely ossified bone structures [212]. However, it must also be noted that there will be a compromise between added design complexity and AM fabrication feasibility – for example, pore diameters must exceed a critical threshold to allow for the full removal of residual particles present during the build process. Furthermore, a more complete understanding of the differences between conventional and AM fabrication in terms of safety is required before many of these advances can be widely applied in the clinic.

On the other side of the operating table, AM proves invaluable for surgical planning. Surgeons plan for implantation by using multiple sources of 2D patient data (e.g. X-rays and CT images), and compile them to create a surgery strategy [213]. With the advent of AM, exact replicas of custom implants can be made (in medical grade polymers if not metals) and used to optimize the surgical planning process by providing a visual and tactile aid [204,205], as seen in Figure 17, or even used as a reference to guide the clinician during surgery. This is particularly useful in cases where fracture patterns are complex, or where intra-operation difficulties are expected. Further to this, patient specific instrumentation, e.g. small jigs with holes to guide surgical equipment during sectioning or screw insertion (osteotomy guides), can be made using the same process [204,205]. Despite the invaluable assistance provided by these aids, uptake will be significantly affected by cost. For example, in Australia, while AM surgery guides are widely used, the patient must pay the entire amount of up to AUD$2000, without any rebates from Medicare (publicly funded health care in Australia) [204]. Whether the significant costs incurred by relatively small populations of vulnerable patients for complicated surgeries, custom implants and patient specific instrumentation will be accounted for in health care systems is as yet uncertain.

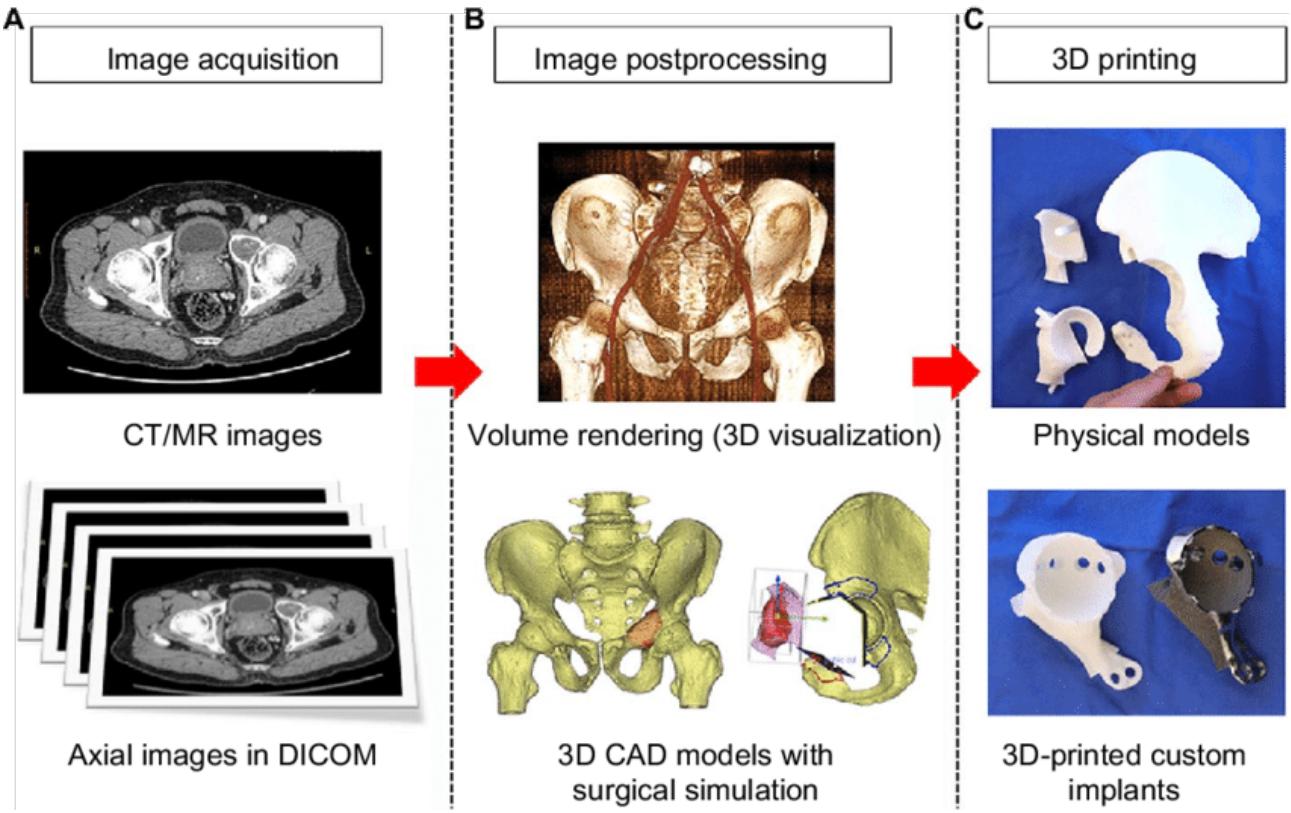

Figure 17 Schematic showing the sequential process of custom implant design and printing showing A) image acquisition, B) image post-processing and CAD modeling, and C) 3D printing of models and custom implants

Reproduced with permission [213], 2016, Dove Press

While the uptake of AM in medicine has been growing exponentially, particularly for vulnerable patients, certain questions and confusions persist regarding the regulation, quality assurance, and intellectual property of customized AM implants. Medical devices in the U.S.A. are classified by the Food and Drug Administration (FDA) based on the risk of the device and/or the levels of control necessary to ensure safety and efficacy; Class I (exempt), Class II (pre-market notification, 510 k pathway) or Class III (high risk, premarket approval pathway) [209,214]. Most orthopedic implants belong to Class III, indicating that these devices may be used in FDA-regulated clinical trials to collect safety and efficacy data prior to receiving approval to market [214,215]. AM techniques pose an interesting dilemma in terms of safety and liability; being that the fabrication technique is the only point of departure from approved devices, many AM implants are treated similarly to

conventionally manufactured implants and require only the application for and reception of patents with finite duration (as well as patient waivers) [216]. This simplistic consideration ignores some of the more pressing issues with AM, particularly in terms of the quality of the customized design, the effects of the build process on part properties and inter-machine variability, even discounting issues that could arise with design features that may impact safety and efficacy. Many simple AM medical devices have reached the American market through the class II pathway, which allows limited use of the device but no commercial marketing without subsequent rigorous testing, and limited numbers have been approved for emergency use [210,216]. However, data on wide-scale testing and comparisons between the properties of conventionally manufactured implants and AM equivalents is not yet available. Long-term data is required to give clinicians and patients a good basis for determining whether AM is likely to provide any benefits over conventional implants with regards to improved functionality and service life. Beyond this, further issues arise with privacy and patents. Is the dissemination of patient-specific designs/models for surgical training or education an assault on said patient's right to privacy? Should the design produced for a specific patient be treated as the intellectual property of the patient or the designer, or even that of the machine technician? This current lack of clarity is likely to deter the involvement of manufacturing companies, and may prove a challenge too burdensome for individual hospitals [217].

The present excitement around focus on custom implants is perhaps overly optimistic, and obscures some of the more pertinent issues regarding 3D printing. While multiple miracle cases have been reported in the media (see [218–220]), the reality of patient-specific implants is altogether murkier. At present, the literature contains less than 5 systematic *in vivo* comparisons between AM fabricated implants and conventionally fabricated implants. Apart from the significant regulatory issues discussed previously, there will likely be significant pushback from clinicians - at present, the quality of conventionally manufactured implants is near perfect, and plenty of long term data is

available. No such easily comparable data is available for AM implants as yet. Little data is available on how quality is controlled, particularly outside the jurisdiction of the FDA in the U.S.A. Consequently, from a clinician's perspective, certain questions must be answered prior to wider uptake;

- Is it worthwhile to produce implants through AM, given that very little long-term usage data exists? Is the current data indicative of actual performance based on the specifics of the surgery, or of long-term performance?
- How will AM change the practices of individual doctors/surgeons – will it be cheaper and/or comparable to conventionally-produced implants? Is it worthwhile to try new technologies, when the risks associated with the implementation of new technologies may be significant? Will willing surgeons be matched with willing patients given that current medical insurance policies are unlikely to cover many of the significant associated costs?
- What quality regulation and legislation is in place, or is possible? How are reproducibility, quality and properties assured? Is the technology scalable to large numbers of patients?
- Can AM implants provide added functionality, for example through longer service lives, increased osteogenic activity, or contain reservoirs with controlled release biologics or therapeutics? What design features to improve implant function are being developed?
- What breakdown products may be produced as compared to conventionally manufactured implants? How will these be excreted? Is the implant likely to cause any inflammatory reactions?
- What are the specific properties (wear, tensile strength, corrosion resistance), and how will these change over time?
- What sterilization methods can be used?

7. An engineering perspective

The International Organization for Standardization and ASTM International define additive manufacturing to be “the process of joining materials to make parts or objects from 3D model data, usually layer upon layer, as opposed to subtractive manufacturing methodologies (ISO 17296 and ASTM F2792) [146]. A workflow for the fabrication and implantation of customized orthopedic implants occurs generally as follows [146,212], noting that some aspects of the workflow below are under present revision;

- Patient data is obtained via X-Ray and CT imaging, and converted into DICOMS
- CAD software is used to join and modify the DICOMs with standard implant designs, as well as design any required patient specific instrumentation (with input from surgeons). Triangulation converts this geometry to an external closed surface, and this is converted into an STL file that describes to designed component to distinguish between inside/outside surfaces. Depending on the complexity of the implant, and the requirement for internal detail or free space, conversion may introduce errors such as surface non-unions or facet degeneration, and these can generally be repaired using CAD.
- The file is processed prior to printing to allow for the specification of build orientation, the generation of support structures and the slicing of the 3D design into layers.
- Net shape production via SLM or EBM occurs, notably process parameters such as laser power and scan speed must be carefully chosen to ensure that the build is successful. Alternatively, near net shape production may occur via DLD production.
- Following printing, the parts may be post-processed to relieve residual stress or heat treatment, and if applicable may be subjected to hot isostatic pressing for densification. Furthermore, surface machining may be carried out to smooth, roughen or otherwise modify

implant surfaces, which may include the application of coatings (e.g. antimicrobial). Following sterilization, the implant may be inserted. Numerous copies of each implant can be produced to allow for sizing trials or surgical planning – these copies may be made using alternate AM techniques (e.g. polymer jetting) to reduce costs.

The progression from design to implantation requires the consideration of multiple factors, including but not limited to patient-specific issues (atypical bone anatomy, quality of bone stock, age and life expectancy) and process-specific issues (intra-machine variation, dimensional tolerances, complexity of design features requiring significant post-processing). As discussed in the previous section, the regulatory legislation for this process must take into account six major aspects affecting implant quality; equipment, material, production, batch, part and finishing [146]. Current regulations are summarized in Figure 18. These can be linked successfully by good thermal management - sensor concepts can be used to monitor intra-process signals such as reflected laser light and melt pool temperature.

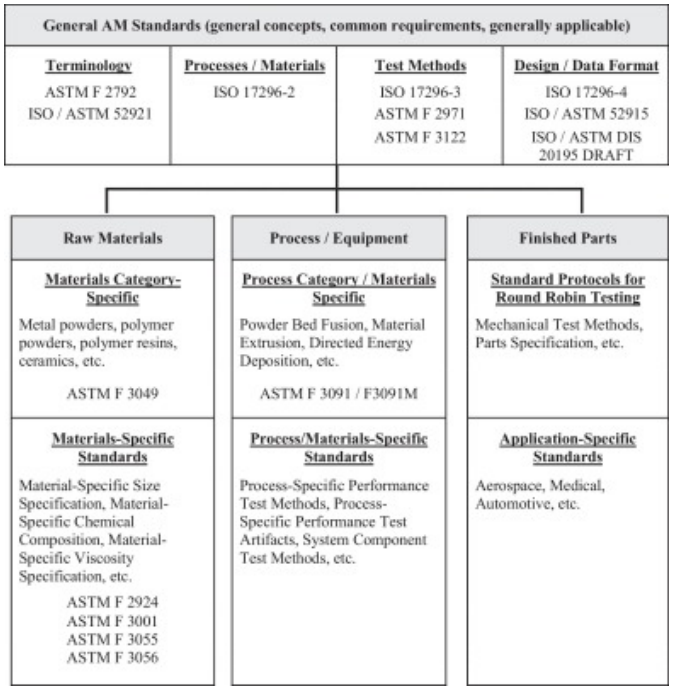

Figure 18 Summary of the ASTM and ISO standards relevant to each stage of producing a customized implant through additive manufacturing.

Reproduced with permission [210], 2016, Elsevier

The most important issue in successful AM implant fabrication is satisfactory design. With new design freedoms come unique design restrictions, discussed briefly here [146,212]. To ensure the even distribution of thermal energy, part cross-sections should be larger at the bottom than at the top, if not constant – this can be achieved through intrinsic design, or through altering build orientation. Sharp edges should be avoided to reduce form defects, as should enclosed pores, as post-process powder removal would not be possible. Finally, overhangs of more than 45º from the vertical should be minimized or supported, as the build-up of thermal stresses can cause the part to warp.

Much research has been conducted into the optimization of AM techniques to produce highly effective orthopedic implants. However, significant gaps remain in the literature with respect to the interplay of various process parameters in the final properties of parts – scan speed, laser power and layer thickness are the most commonly investigated process parameters. Multiple adjacent factors must also be fully understood for effective implant design, fabrication and usage, including but not limited to; the influence of powder feed rate in DLD, oxygen pick-up in EBM, and the replication of bone features of multiple length scales (osteons, lamellae and collage fibers) [60,70,128]. The development of strategies to reduce residual stresses during fabrication is of paramount importance, as is the quantification of processing strategies to produce tailored porosity, surface roughness and bulk properties. Of particular interest is the development of weight reducing lattice structures within orthopedic implants, which can both reduce modulus mismatch and improve host responses.

8. Summary

Titanium and its alloys have proven to be a model material for orthopedic implants, aided by evident bio-inertness and low cytotoxicity; whilst readily produced by numerous AM production routes. Techniques such as SLM, EBM and DLD have been used widely in the research and

development of customized orthopedic implants, with parts produced behaving comparably to implants produced from wrought material. The properties of parts produced by each technique are variable based on the specific process parameters used, but certain generalizations can be made as follows – SLM has greater possible scan rates and thus cooling rates than EBM, and so SLM parts generally have greater fractions of α'phases as compared to EBM parts which have α lamellae and β phases in their microstructures. This affects their mechanical properties - parts produced by SLM generally have higher surface roughness, porosity and residual stress, but also higher tensile strength. Porosity is observed between layers in SLM parts, while at the laser turning point in EBM parts. The amount of porosity produced in SLM and EBM parts generally requires the application of hot isostatic processing post-build to closer the pores and increase the fatigue strength. SLM parts will have higher fracture strengths but correspondingly lower ductility than EBM parts. The energy efficiency and build time minimization of EBM is better than that of SLM. DLD parts have the highest surface roughness and structural inhomogeneity of all three techniques, and generally require post-processing to reduce microstructural inhomogeneity. However, compositional gradients may be formed with this technique leading to the possibility of functional variation. Research into the optimization of process parameters (all three techniques) for orthopedic applications is as yet in its early stages, as the bulk of research into mechanical properties and surfaces has been from the perspective of aerospace and industrial applications.

Further to the new possibilities offered by AM fabrication, new alloy compositions are also of great interest in improving orthopedic implant functionality. The continued development of lower modulus β-Ti alloys shows great promise in matching bone tissue. Compositions such as Ti-35Nb-7Zr-5Ta and Ti-29Nb-13Ta-4.6Zr with moduli between 40 and 80 GPa are suited to production by additive manufacturing. The rate-limiting aspect of utilizing these new alloys in the AM of orthopedic implants is the difficulty in producing feed-stock suitable for SLM, EBM or DLD.

Powder production is still limited to a handful of companies worldwide. Similarly, improvements in computing power and software capabilities will further improve the translation of DICOMs to patient-specific implants and instrumentation.

Many post-processing techniques have been widely investigated for the further functionalization of AM Ti-based orthopedic implants, including the use of heat treatment, surface patterning and the application of coatings. Surface modifications such as roughening through physical, chemical or biochemical methods, as well as coatings incorporating calcium phosphate-based ceramics or bio-active elements such as Sr will further improve the effectiveness of Ti-based orthopedic implants.

Presently, AM has the potential to improve upon conventional fabrication techniques, particularly in the production of low volumes of highly complex parts. This is already invaluable for vulnerable patients, and going forward, the increased uptake of AM orthopedic implants and PSI has the potential to improve patient outcomes. Considerable research has been conducted into the efficacy of SLM, EBM and DLD as fabrication techniques for orthopedic implants. Properties comparable to conventional Ti implants have been produced, however, currently all evidence as to efficacy is in its infancy – long term performance has not yet been studied extensively. As the understanding of these techniques develops, further tailoring and customization for specific types of implants can be implemented. This is the current state of the field, and significant advances are expected in the next ten years.

Acknowledgements

Thanks to Emily Massahud and Tiphaine Bazin for fruitful discussions and encouragement.

NB is supported by Woodside Energy.

Received: ((will be filled in by the editorial staff))
Revised: ((will be filled in by the editorial staff))
Published online: ((will be filled in by the editorial staff))

References

[1] A. J. R. Registry, *Third AJRR Annual Report on Hip and Knee Arthroplasty Data*, Rosemont, **2016**.

[2] B. M. Holzapfel, J. C. Reichert, J. T. Schantz, U. Gbureck, L. Rackwitz, U. Nöth, F. Jakob, M. Rudert, J. Groll, D. W. Hutmacher, *Adv. Drug Deliv. Rev.* **2013**, *65*, 581.

[3] M. Long, H. . Rack, *Biomaterials* **1998**, *19*, 1621.

[4] L. Linder, A. Carlsson, L. Marsal, L. M. Bjursten, P. I. Brånemark, *J. Bone Joint Surg. Br.* **1988**, *70*, 550.

[5] M. Geetha, A. K. Singh, R. Asokamani, A. K. Gogia, *Prog. Mater. Sci.* **2009**, *54*, 397.

[6] L. Feller, Y. Jadwat, R. A. G. Khammissa, R. Meyerov, I. Schechter, J. Lemmer, *Biomed Res. Int.* **2015**, *2015*, 1.

[7] M. Browne, P. J. Gregson, *Biomaterials* **1994**, *15*, 894.

[8] H. Matsuno, A. Yokoyama, F. Watari, M. Uo, T. Kawasaki, *Biomaterials* **2001**, *22*, 1253.

[9] A. Sidambe, *Materials (Basel).* **2014**, *7*, 8168.

[10] V. S. de Viteri, E. Fuentes, in *Tribol. - Fundam. Adv.* (Ed.: J. Gegner), InTech Open, **2013**.

[11] M. Peters, J. Hemptenmacher, J. Kumpfert, C. Leyens, *Structure and Properties of Titanium and Titanium Alloys*, **2003**.

[12] M. Peters, C. Leyens, D. L. R. German, **2003**, 245.

[13] F. Yu, O. Addison, A. J. Davenport, *Acta Biomater.* **2015**, *26*, 355.

[14] P. Fox, S. Pogson, C. J. Sutcliffe, E. Jones, *Surf. Coatings Technol.* **2008**, *202*, 5001.

[15] A. Nouri, P. D. Hodgson, C. Wen, **2010**, 415.

[16] S. Nag, R. Banerjee, H. L. Fraser, *Acta Biomater.* **2007**, *3*, 369.

[17] V. Brailovski, S. Prokoshkin, M. Gauthier, K. Inaekyan, S. Dubinskiy, *J. Alloys Compd.* **2013**, *577*, S413.

[18] F. Y. Zhou, B. L. Wang, K. J. Qiu, W. J. Lin, L. Li, Y. B. Wang, F. L. Nie, Y. F. Zheng, *Mater. Sci. Eng. C* **2012**, *32*, 851.

[19] S. Ozan, J. Lin, Y. Li, R. Ipek, C. Wen, *Acta Biomater.* **2015**, *20*, 176.

[20] C. Oldani, A. Dominguez, *Recent Adv. Arthroplast.* **2012**, 149.

[21] L. De Nardo, G. Raffaini, E. Ebramzadeh, F. Ganazzoli, *Int. J. Artif. Organs* **2012**, *35*, 629.

[22] S. Nag, R. Banerjee, in *ASM Handb.* (Ed.: R. Narayan), ASM International, **2012**, pp. 6–16.

[23] J. Breme, E. Eisenbarth, V. Biehl, in *Titan. Titan. Alloy. Fundam. Appl.* (Eds.: C. Leyens, M. Peters), WILEY-VCH Verlag GmbH & Co. KGaA, Weinheim, **2003**, pp. 423–451.

[24] E. Sallica-Leva, A. L. Jardini, J. B. Fogagnolo, *J. Mech. Behav. Biomed. Mater.* **2013**, *26*, 98.

[25] P. Heinl, C. Körner, R. F. Singer, *Adv. Eng. Mater.* **2008**, *10*, 882.

[26] G. E. Ryan, A. S. Pandit, D. P. Apatsidis, *Biomaterials* **2008**, *29*, 3625.

[27] A. Basalah, Y. Shanjani, S. Esmaeili, E. Toyserkani, *J. Biomed. Mater. Res. - Part B Appl. Biomater.* **2012**, *100 B*, 1970.

[28] M. Tamaddon, J. T. Czernuszka, *Hard Tissue* **2013**, *2*, 1.

[29] S. Sobieszczyk, *Adv. Mater. Sci.* **2010**, *10*, 20.

[30] L. Ponsonnet, K. Reybier, N. Jaffrezic, V. Comte, C. Lagneau, M. Lissac, C. Martelet, *Mater. Sci. Eng. C* **2003**, *23*, 551.

[31] M. Bigerelle, K. Anselme, B. Noel, I. Ruderman, P. Hardouin, A. Iost, *Biomaterials* **2002**, *23*, 1563.

[32] J. Fu, Y. Hu, Z. Guo, Y. Zhang, Y. Hao, S. Li, *Appl. Surf. Sci.* **2008**, *255*, 286.

[33] T. P. Kunzler, T. Drobek, M. Schuler, N. D. Spencer, *Biomaterials* **2007**, *28*, 2175.

[34] F. C. Fierz, F. Beckmann, M. Huser, S. H. Irsen, B. Leukers, F. Witte, Ö. Degistirici, A. Andronache, M. Thie, B. Müller, *Biomaterials* **2008**, *29*, 3799.

[35] A. Koptyug, C. Bergemann, R. Lange, V. E. Jaggi, L. E. Rännar, J. B. Nebe, in *Mater. Sci. Forum*, Trans Tech Publications, **2014**, pp. 1292–1297.

[36] J. Karlsson, A. Snis, H. Engqvist, J. Lausmaa, *J. Mater. Process. Technol.* **2013**, *213*, 2109.

[37] B. Baufeld, O. Van Der Biest, R. Gault, *Mater. Des.* **2010**, *31*, S106.

[38] T. T. Wohlers, W. Associates, *Wohlers Report 2015: Additive Manufacturing and 3D Printing State of the Industry: Annual Worldwide Progress Report*, Wohlers Associates, **2015**.

[39] P. Unwin, *SPIE Photonics West 2014-LASE Lasers Sources* **2014**, *8970*, 897005.

[40] B. P. Conner, G. P. Manogharan, A. N. Martof, L. M. Rodomsky, C. M. Rodomsky, D. C. Jordan, J. W. Limperos, *Addit. Manuf.* **2014**, *1-4*, 64.

[41] H. Miura, *KONA Powder Part. J.* **2015**, *32*, 253.

[42] J. U. Pucci, B. R. Christophe, J. A. Sisti, E. S. Connolly, *Biotechnol. Adv.* **2017**, *35*, 521.

[43] D. Beski, T. Dufour, F. Gelaude, A. Ilankovan, M. Kvasnytsia, M. Lawrenchuk, I. Lukyanenko, M. Mir, L. Neumann, A. Nguyen, A. Soares, E. Sauvage, K. Vanderperren, D. Vangeneugden, *Software for Biofabrication*, Elsevier Inc., **2015**.

[44] L. E. Murr, S. M. Gaytan, F. Medina, H. Lopez, E. Martinez, B. I. Machado, D. H. Hernandez, L. Martinez, M. I. Lopez, R. B. Wicker, J. Bracke, *Philos. Trans. A. Math. Phys. Eng. Sci.* **2010**, *368*, 1999.

[45] B. Vandenbroucke, J.-P. Kruth, *Rapid Prototyp. J.* **2007**, *13*, 196.

[46] T. M. Mower, M. J. Long, *Mater. Sci. Eng. A* **2016**, *651*, 198.

[47] V. Cain, L. Thijs, J. Van Humbeeck, B. Van Hooreweder, R. Knutsen, *Addit. Manuf.* **2014**, *5*, 68.

[48] M. a. Fernandez-Yague, S. A. Abbah, L. McNamara, D. I. Zeugolis, A. Pandit, M. J. Biggs, *Adv. Drug Deliv. Rev.* **2015**, *84*, 1.

[49] X. Wu, J. Liang, J. Mei, C. Mitchell, P. S. Goodwin, W. Voice, *Mater. Des.* **2004**, *25*, 137.

[50] L. E. Murr, E. Martinez, K. N. Amato, S. M. Gaytan, J. Hernandez, D. a. Ramirez, P. W. Shindo, F. Medina, R. B. Wicker, *J. Mater. Res. Technol.* **2012**, *1*, 42.

[51] Q. C. Liu, J. Elambasseril, S. J. Sun, M. Leary, M. Brandt, P. K. Sharp, *Adv. Mater. Res.* **2014**, *891-892*, 1519.

[52] S. Leuders, M. Thöne, A. Riemer, T. Niendorf, T. Tröster, H. A. a. Richard, H. J. J. Maier, *Int. J. Fatigue* **2013**, *48*, 300.

[53] M. N. Ahsan, A. J. Pinkerton, R. J. Moat, J. Shackleton, in *Mater. Sci. Eng. A*, **2011**, pp. 7648–7657.

[54] T. Marcu, C. Menapace, L. Girardini, D. Leordean, C. Popa, *Rapid Prototyp. J.* **2014**, *20*,

301.

[55] D. K. Pattanayak, A. Fukuda, T. Matsushita, M. Takemoto, S. Fujibayashi, K. Sasaki, N. Nishida, T. Nakamura, T. Kokubo, *Acta Biomater.* **2011**, *7*, 1398.

[56] I. Yadroitsev, P. Krakhmalev, I. Yadroitsava, *J. Alloys Compd.* **2014**, *583*, 404.

[57] J. Romano, L. Ladani, J. Razmi, M. Sadowski, *Addit. Manuf.* **2015**, *8*, 1.

[58] M. Simonelli, Y. Y. Tse, C. Tuck, *J. Phys. Conf. Ser.* **2012**, *371*, 012084.

[59] M. Speirs, J. Van Humbeeck, J. Schrooten, J. Luyten, J. P. Kruth, *Procedia CIRP* **2013**, *5*, 79.

[60] A. Butscher, M. Bohner, S. Hofmann, L. Gauckler, R. Müller, *Acta Biomater.* **2011**, *7*, 907.

[61] W. Xue, B. V. Krishna, A. Bandyopadhyay, S. Bose, *Acta Biomater.* **2007**, *3*, 1007.

[62] A. El-Hajje, E. C. Kolos, J. K. Wang, S. Maleksaeedi, Z. He, F. E. Wiria, C. Choong, A. J. Ruys, *J. Mater. Sci. Mater. Med.* **2014**, 2471.

[63] V. Guneta, J. K. Wang, S. Maleksaeedi, Z. M. He, M. T. C. Wong, C. Choong, *J. Biomimetics, Biomater. Biomed. Eng.* **2014**, *21*, 101.

[64] S. C. Cox, J. A. Thornby, G. J. Gibbons, M. A. Williams, K. K. Mallick, *Mater. Sci. Eng. C. Mater. Biol. Appl.* **2015**, *47*, 237.

[65] A. Butscher, M. Bohner, N. Doebelin, S. Hofmann, R. Müller, *Acta Biomater.* **2013**, *9*, 9149.

[66] S. L. Sing, J. An, W. Y. Yeong, F. E. Wiria, *J. Orthop. Res.* **2016**, *34*, 369.

[67] L. E. Murr, *Addit. Manuf.* **2014**, *5*, 40.

[68] L. E. Murr, S. A. Quinones, S. M. Gaytan, M. I. Lopez, A. Rodela, E. Y. Martinez, D. H. Hernandez, E. Martinez, F. Medina, R. B. Wicker, *J. Mech. Behav. Biomed. Mater.* **2009**, *2*, 20.

[69] H. Gong, K. Rafi, H. Gu, T. Starr, B. Stucker, *Addit. Manuf.* **2014**, *1-4*, 87.

[70] K. S. Munir, Y. Li, C. Wen, *Met. Foam Bone Process. Modif. Charact. Prop.* **2016**, 1.

[71] S. Zhang, X. Cheng, Y. Yao, Y. Wei, C. Han, Y. Shi, Q. Wei, Z. Zhang, *Mater. Sci. Eng. C* **2015**, *53*, 50.

[72] P. Hanzl, M. Zetek, T. Bakša, T. Kroupa, *Procedia Eng.* **2015**, *100*, 1405.

[73] A. M. Khorasani, I. Gibson, M. Goldberg, G. Littlefair, *Mater. Des.* **2016**, *103*, 348.

[74] T. Amine, J. W. Newkirk, F. Liou, *Case Stud. Therm. Eng.* **2014**, *3*, 21.

[75] C. Qiu, N. J. E. Adkins, M. M. Attallah, *Mater. Sci. Eng. A* **2013**, *578*, 230.

[76] D. Leordean, S. a. Radu, D. Frățilă, P. Berce, *Int. J. Adv. Manuf. Technol.* **2015**, DOI 10.1007/s00170-015-6873-0.

[77] T. Marcu, M. Todea, L. Maines, D. Leordean, P. Berce, C. Popa, *Powder Metall.* **2012**, *55*, 309.

[78] D. A. Hollander, M. von Walter, T. Wirtz, R. Sellei, B. Schmidt-Rohlfing, O. Paar, H.-J. Erli, *Biomaterials* **2006**, *27*, 955.

[79] P. H. Warnke, T. Douglas, P. Wollny, E. Sherry, M. Steiner, S. Galonska, S. T. Becker, I. N. Springer, J. Wiltfang, S. Sivananthan, *Tissue Eng. Part C Methods* **2009**, *15*, 115.

[80] C. Mangano, A. Piattelli, S. d'Avila, G. Iezzi, F. Mangano, T. Onuma, J. A. Shibli, *J. Oral Implantol.* **2010**, *36*, 91.

[81] S. Van Bael, Y. C. Chai, S. Truscello, M. Moesen, G. Kerckhofs, H. Van Oosterwyck, J. P.

Kruth, J. Schrooten, *Acta Biomater.* **2012**, *8*, 2824.

[82] A. Shaoki, J. Xu, H. Sun, X. Chen, J. Ouyang, X. Zhuang, F. Deng, *Biofabrication* **2016**, *8*, 045014.

[83] N. Hrabe, T. Quinn, *Mater. Sci. Eng. A* **2013**, *573*, 271.

[84] D. Herzog, V. Seyda, E. Wycisk, C. Emmelmann, *Acta Mater.* **2016**, DOI 10.1016/j.actamat.2016.07.019.

[85] X. P. Tan, Y. J. Tan, C. S. L. Chow, S. B. Tor, W. Y. Yeong, *Mater. Sci. Eng. C* **2017**, *76*, 1328.

[86] S. Ponader, C. Von Wilmowsky, M. Widenmayer, R. Lutz, P. Heinl, C. Körner, R. F. Singer, E. Nkenke, F. W. Neukam, K. A. Schlegel, *J. Biomed. Mater. Res. - Part A* **2010**, *92*, 56.

[87] C. Guo, W. Ge, F. Lin, *J. Mater. Process. Technol.* **2015**, *217*, 148.

[88] M. Seifi, M. Dahar, R. Aman, O. Harrysson, J. Beuth, J. J. Lewandowski, *Jom* **2015**, *67*, 597.

[89] X. Tan, Y. Kok, Y. J. Tan, M. Descoins, D. Mangelinck, S. B. Tor, K. F. Leong, C. K. Chua, *Acta Mater.* **2015**, *97*, 1.

[90] A. A. Antonysamy, J. Meyer, P. B. Prangnell, *Mater. Charact.* **2013**, *84*, 153.

[91] J. Karlsson, M. Norell, U. Ackelid, H. Engqvist, J. Lausmaa, *J. Manuf. Process.* **2015**, *17*, 120.

[92] G. Chahine, M. Koike, T. Okabe, P. Smith, R. Kovacevic, *Jom* **2008**, *60*, 50.

[93] W. Xia, C. Lindahl, J. Lausmaa, H. Engqvist, **2011**.

[94] L. T. Duarte, S. R. Biaggio, R. C. Rocha-Filho, N. Bocchi, *Corros. Sci.* **2013**, *72*, 35.

[95] X. Bin Su, Y. Q. Yang, P. Yu, J. F. Sun, *Trans. Nonferrous Met. Soc. China (English Ed.* **2012**, *22*, s181.

[96] B. Song, S. Dong, B. Zhang, H. Liao, C. Coddet, *Mater. Des.* **2012**, *35*, 120.

[97] J. W. Park, Y. J. Kim, J. H. Jang, *Clin. Oral Implants Res.* **2010**, *21*, 398.

[98] P. Edwards, M. Ramulu, *Mater. Sci. Eng. A* **2014**, *598*, 327.

[99] D. H. Abdeen, B. R. Palmer, *Rapid Prototyp. J.* **2016**, *22*, 609.

[100] S. Ponader, E. Vairaktaris, P. Heinl, C. V. Wilmowsky, A. Rottmair, C. Körner, R. F. Singer, S. Holst, K. A. Schlegel, F. W. Neukam, E. Nkenke, *J. Biomed. Mater. Res. - Part A* **2008**, *84*, 1111.

[101] P. Thomsen, J. Malmstrom, L. Emanuelsson, M. Rene, A. Snis, J. Malmstro, L. Emanuelsson, M. Rene, A. Snis, J. Malmström, L. Emanuelsson, M. René, A. Snis, *J. Biomed. Mater. Res. B. Appl. Biomater.* **2009**, *90 B*, 35.

[102] A. Palmquist, A. Snis, L. Emanuelsson, M. Browne, P. Thomsen, *J. Biomater. Appl.* **2013**, *27*, 1003.

[103] J. Lv, Z. Jia, J. Li, Y. Wang, J. Yang, P. Xiu, K. Zhang, H. Cai, Z. Liu, *Adv. Eng. Mater.* **2015**, n/a.

[104] C. M. Haslauer, J. C. Springer, O. L. A. Harrysson, E. G. Loboa, N. A. Monteiro-Riviere, D. J. Marcellin-Little, *Med. Eng. Phys.* **2010**, *32*, 645.

[105] N. Shamsaei, A. Yadollahi, L. Bian, S. M. Thompson, *Addit. Manuf.* **2015**, *8*, 12.

[106] R. Vilar, in *Compr. Mater. Process.* (Ed.: S. Hashmi), Elsevier, **2014**, pp. 163–216.

[107] M. Polanski, M. Kwiatkowska, I. Kunce, J. Bystrzycki, *Int. J. Hydrogen Energy* **2013**, *38*,

12159.

[108] V. K. Balla, P. D. DeVasConCellos, W. Xue, S. Bose, A. Bandyopadhyay, *Acta Biomater.* **2009**, *5*, 1831.

[109] R. Banerjee, P. C. Collins, D. Bhattacharyya, S. Banerjee, H. L. Fraser, *Acta Mater.* **2003**, *51*, 3277.

[110] R. Banerjee, S. Nag, H. L. Fraser, *Mater. Sci. Eng. C* **2005**, *25*, 282.

[111] M. A. Larosa, A. L. Jardini, L. F. Bernardes, M. R. Wolf Maciel, R. Maciel Filho, C. A. C. Zaváglia, F. Zaváglia, D. R. Calderoni, P. Kharmandayan, in *High Value Manuf. Adv. Res. Virtual Rapid Prototyp. - Proc. 6th Int. Conf. Adv. Res. Rapid Prototyping, VR@P 2013*, **2014**, pp. 297–301.

[112] E. C. Santos, M. Shiomi, K. Osakada, T. Laoui, *Int. J. Mach. Tools Manuf.* **2006**, *46*, 1459.

[113] K. Zhang, W. Liu, X. Shang, *Opt. Laser Technol.* **2007**, *39*, 549.

[114] A. Suárez, M. J. Tobar, A. Yáñez, I. Pérez, J. Sampedro, V. Amigó, J. J. Candel, *Phys. Procedia* **2011**, *12*, 666.

[115] S. M. Thompson, L. Bian, N. Shamsaei, A. Yadollahi, *Addit. Manuf.* **2015**, *8*, 36.

[116] A. J. Sterling, B. Torries, N. Shamsaei, S. M. Thompson, D. W. Seely, *Mater. Sci. Eng. A* **2016**, *655*, 100.

[117] M. Gharbi, P. Peyre, C. Gorny, M. Carin, S. Morville, P. Le Masson, D. Carron, R. Fabbro, *J. Mater. Process. Technol.* **2013**, *213*, 791.

[118] A. Sterling, N. Shamsaei, B. Torries, S. M. Thompson, *Procedia Eng.* **2015**, *133*, 576.

[119] S. Palanivel, A. K. Dutt, E. J. Faierson, R. S. Mishra, *Mater. Sci. Eng. A* **2016**, *654*, 39.

[120] R. P. Mulay, J. A. Moore, J. N. Florando, N. R. Barton, M. Kumar, *Mater. Sci. Eng. A* **2016**, *666*, 43.

[121] P. A. Kobryn, S. L. Semiatin, *J. Mater. Process. Technol.* **2003**, *135*, 330.

[122] X. Wu, J. Liang, J. Mei, C. Mitchell, P. S. S. Goodwin, W. Voice, *Mater. Des.* **2004**, *25*, 137.

[123] C. Qiu, G. A. Ravi, C. Dance, A. Ranson, S. Dilworth, M. M. Attallah, *J. Alloys Compd.* **2015**, *629*, 351.

[124] J. S. Keist, T. A. Palmer, *Mater. Des.* **2016**, *106*, 482.

[125] A. Bandyopadhyay, F. Espana, V. K. Balla, S. Bose, Y. Ohgami, N. M. Davies, *Acta Biomater.* **2010**, *6*, 1640.

[126] X. Li, Y. F. Feng, C. T. Wang, G. C. Li, W. Lei, Z. Y. Zhang, L. Wang, *PLoS One* **2012**, *7*, 1.

[127] X. Zhao, S. Li, M. Zhang, Y. Liu, T. B. Sercombe, S. Wang, Y. Hao, R. Yang, L. E. Murr, *Mater. Des.* **2016**, *95*, 21.

[128] P. Li, D. H. Warner, A. Fatemi, N. Phan, *Int. J. Fatigue* **2016**, *85*, 130.

[129] J. Günther, D. Krewerth, T. Lippmann, S. Leuders, T. Tröster, A. Weidner, H. Biermann, T. Niendorf, *Int. J. Fatigue* **2017**, *94*, 236.

[130] S. Bagehorn, J. Wehr, H. J. Maier, *Int. J. Fatigue* **2017**, *102*, 135.

[131] Y. Zhai, D. A. Lados, E. J. Brown, G. N. Vigilante, *Int. J. Fatigue* **2016**, *93*, 51.

[132] K. F. Walker, Q. Liu, M. Brandt, *Int. J. Fatigue* **2017**, *104*, 302.

[133] Y. Zhai, H. Galarraga, D. A. Lados, in *Procedia Eng.*, Elsevier, **2015**, pp. 658–666.

[134] H. Wang, B. Zhao, C. Liu, C. Wang, X. Tan, M. Hu, *PLoS One* **2016**, *11*, 1.

[135] M. Niinomi, M. Nakai, J. Hieda, *Acta Biomater.* **2012**, *8*, 3888.

[136] M. Niinomi, *Mater. Sci. Eng. A* **1998**, *243*, 231.

[137] L. M. Elias, S. G. Schneider, S. Schneider, H. M. Silva, F. Malvisi, *Mater. Sci. Eng. A* **2006**, *432*, 108.

[138] B. Vrancken, L. Thijs, J.-P. Kruth, J. Van Humbeeck, *Acta Mater.* **2014**, *68*, 150.

[139] Y. Zhou, S. F. Wen, B. Song, X. Zhou, Q. Teng, Q. S. Wei, Y. S. Shi, *Mater. Des.* **2016**, *89*, 1199.

[140] J. M. Calderon-Moreno, C. Vasilescu, S. I. Drob, S. Ivanescu, P. Osiceanu, P. Drob, M. Popa, S. Preda, E. Vasilescu, *J. Alloys Compd.* **2014**, *612*, 398.

[141] S. Samuel, S. Nag, S. Nasrazadani, V. Ukirde, M. El Bouanani, A. Mohandas, K. Nguyen, R. Banerjee, *J. Biomed. Mater. Res. - Part A* **2010**, *94*, 1251.

[142] E. Eisenbarth, D. Velten, M. Müller, R. Thull, J. Breme, *Biomaterials* **2004**, *25*, 5705.

[143] M. T. Mohammed, Z. A. Khan, M. Geetha, A. N. Siddiquee, *J. Alloys Compd.* **2015**, *634*, 272.

[144] Q. Meng, S. Guo, Q. Liu, L. Hu, X. Zhao, *Prog. Nat. Sci. Mater. Int.* **2014**, *24*, 157.

[145] L. Nie, Y. Zhan, T. Hu, X. Chen, C. Wang, *J. Mech. Behav. Biomed. Mater.* **2014**, *29*, 1.

[146] M. Schmidt, M. Merklein, D. Bourell, D. Dimitrov, T. Hausotte, K. Wegener, L. Overmeyer, F. Vollertsen, G. N. Levy, *CIRP Ann. - Manuf. Technol.* **2017**, *66*, 561.

[147] B. Engel, D. L. Bourell, *Rapid Prototyp. J.* **2000**, *6*, 97.

[148] Y. Y. Sun, S. Gulizia, C. H. Oh, C. Doblin, Y. F. Yang, M. Qian, *Jom* **2015**, *67*, 564.

[149] H. P. Tang, J. Wang, M. Qian, *A Perspective on the Future of Titanium Powder Metallurgy*, Elsevier, **2015**.

[150] H. P. Tang, M. Qian, N. Liu, X. Z. Zhang, G. Y. Yang, J. Wang, *Jom* **2015**, *67*, 555.

[151] Z. Zhang, L. Yuan, P. D. Lee, E. Jones, J. R. Jones, *J. Biomed. Mater. Res. - Part B Appl. Biomater.* **2014**, *102*, 1689.

[152] S. Maleksaeedi, J. K. Wang, A. El-Hajje, L. Harb, V. Guneta, Z. He, F. E. Wiria, C. Choong, A. J. Ruys, in *Procedia CIRP*, **2013**, pp. 158–163.

[153] T. B. Kim, S. Yue, Z. Zhang, E. Jones, J. R. Jones, P. D. Lee, *J. Mater. Process. Technol.* **2014**, *214*, 2706.

[154] S. Arabnejad, B. Johnston, M. Tanzer, D. Pasini, *J. Orthop. Res.* **2017**, *35*, 1774.

[155] F. Calignano, *Mater. Des.* **2014**, *64*, 203.

[156] M. X. Gan, C. H. Wong, *J. Mater. Process. Technol.* **2016**, *238*, 474.

[157] A. Hussein, L. Hao, C. Yan, R. Everson, P. Young, *J. Mater. Process. Technol.* **2013**, *213*, 1019.

[158] G. Strano, L. Hao, R. M. Everson, K. E. Evans, *Int. J. Adv. Manuf. Technol.* **2013**, *66*, 1247.

[159] K. Zeng, D. Pal, C. Teng, B. E. Stucker, *Addit. Manuf.* **2015**, *6*, 67.

[160] D. Frank, G. Fadel, *J. Intell. Manuf.* **1995**, *6*, 339.

[161] B. Vrancken, L. Thijs, J.-P. Kruth, J. Van Humbeeck, *J. Alloys Compd.* **2012**, *541*, 177.

[162] E. Brandl, D. Greitemeier, *Mater. Lett.* **2012**, *81*, 84.

[163] J. I. Rosales-Leal, M. A. Rodríguez-Valverde, G. Mazzaglia, P. J. Ramón-Torregrosa, L. Díaz-Rodríguez, O. García-Martínez, M. Vallecillo-Capilla, C. Ruiz, M. A. Cabrerizo-Vílchez, *Colloids Surfaces A Physicochem. Eng. Asp.* **2010**, *365*, 222.

[164] D. . Deligianni, N. Katsala, S. Ladas, D. Sotiropoulou, J. Amedee, Y. . Missirlis, *Biomaterials* **2001**, *22*, 1241.

[165] B. D. Boyan, T. W. Hummert, D. D. Dean, Z. Schwartz, *Biomaterials* **1996**, *17*, 137.

[166] J. Lincks, B. D. Boyan, C. R. Blanchard, C. H. Lohmann, Y. Liu, D. L. Cochran, D. D. Dean, Z. Schwartz, *Biomater. Silver Jubil. Compend.* **2006**, *19*, 147.

[167] P. Linez-Bataillon, F. Monchau, M. Bigerelle, H. F. Hildebrand, *Biomol. Eng.* **2002**, *19*, 133.

[168] A. Wennerberg, T. Albrektsson, R. Jimbo, *Implant Surfaces and Their Biological and Clinical Impact*, Springer, Berlin, **2015**.

[169] E. Sachs, A. Curodeau, D. Gossard, H. Jee, M. Cima, S. Caldarise, *Solid Free. Fabr. Symp.* **1994**, 56.

[170] H. Shahali, A. Jaggessar, P. K. Yarlagadda, *Procedia Eng.* **2017**, *174*, 1067.

[171] B. G. X. Zhang, D. E. Myers, G. G. Wallace, M. Brandt, P. F. M. Choong, *Int. J. Mol. Sci.* **2014**, *15*, 11878.

[172] W. Xia, C. Lindahl, J. Lausmaa, P. Borchardt, A. Ballo, P. Thomsen, H. Engqvist, *Acta Biomater.* **2010**, *6*, 1591.

[173] K. Søballe, *Acta Orthop. Scand. Suppl.* **1993**, *255*, 1.

[174] A. Eckardt, H. M. Aberman, H. D. Cantwell, J. Heine, *Arch. Orthop. Trauma Surg.* **2003**, *123*, 28.

[175] B. R. Levine, S. Sporer, R. A. Poggie, C. J. Della Valle, J. J. Jacobs, *Biomaterials* **2006**, *27*, 4671.

[176] D. M. Findlay, K. Welldon, G. J. Atkins, D. W. Howie, A. C. W. Zannettino, D. Bobyn, *Biomaterials* **2004**, *25*, 2215.

[177] Y. Liu, C. Bao, D. Wismeijer, G. Wu, *Mater. Sci. Eng. C* **2015**, *49*, 323.

[178] V. K. Balla, S. Banerjee, S. Bose, A. Bandyopadhyay, *Acta Biomater.* **2010**, *6*, 2329.

[179] N. Harrison, P. E. McHugh, W. Curtin, P. Mc Donnell, *J. Mech. Behav. Biomed. Mater.* **2013**, *21*, 37.

[180] P. Stenlund, O. Omar, U. Brohede, S. Norgren, B. Norlindh, A. Johansson, J. Lausmaa, P. Thomsen, A. Palmquist, *Acta Biomater.* **2015**, *20*, 165.

[181] J. B. Tong, X. Lu, C. C. Liu, L. N. Wang, X. H. Qu, *Jom* **2015**, *67*, 573.

[182] M. T. Vestermark, E.-M. Hauge, K. Soballe, J. E. Bechtold, T. Jakobsen, J. Baas, *Acta Orthop.* **2011**, *82*, 614.

[183] M. Schnabelrauch, A. R. Kautz, J. Weisser, J. Schmidt, A. Henning, C. Schrader, U. Bayer, F. Schlottig, *Eur. Cells Mater.* **2007**, *14*, 91.

[184] J. Yan, Y. Zhang, Y. Han, Y. Zhao, J. Sun, H. Yan, *Zhonghua Kou Qiang Yi Xue Za Zhi* **2010**, *45*, 89.

[185] J. Terra, E. R. Dourado, J.-G. Eon, D. E. Ellis, G. Gonzalez, A. M. Rossi, *Phys. Chem. Chem. Phys.* **2009**, *11*, 568.

[186] M. T. Vestermark, *Dan. Med. Bull.* **2011**, *58*, B4286.

[187] S. Tan, B. Zhang, X. Zhu, P. Ao, H. Guo, W. Yi, G.-Q. Zhou, *Biomed Res. Int.* **2014**, *2014*,

814057.

[188] Z. Saidak, P. J. Marie, *Pharmacol. Ther.* **2012**, *136*, 216.

[189] Y. Li, Q. Li, S. Zhu, E. Luo, J. Li, G. Feng, Y. Liao, J. Hu, *Biomaterials* **2010**, *31*, 9006.

[190] H. Yang, M. Lin, Y. Xu, G. Shang, R. Wang, K. Chen, **2015**, *8*, 257.

[191] J. Vaithilingam, E. Prina, R. D. Goodridge, R. J. M. Hague, S. Edmondson, F. R. A. J. Rose, S. D. R. Christie, *Mater. Sci. Eng. C* **2016**, *67*, 294.

[192] S. C. Cox, P. Jamshidi, N. M. Eisenstein, M. A. Webber, H. Burton, R. J. A. Moakes, O. Addison, M. Attallah, D. E. T. Shepherd, L. M. Grover, *ACS Biomater. Sci. Eng.* **2017**, *3*, 1616.

[193] L. Matouskova, M. Ackermann, J. Horakova, L. Capek, P. Henys, J. Safka, *Expert Rev. Med. Devices* **2018**, *15*, 313.

[194] L. E. J. Thomas-Seale, J. C. Kirkman-Brown, M. M. Attallah, D. M. Espino, D. E. T. Shepherd, *Int. J. Prod. Econ.* **2018**, *198*, 104.

[195] F. L. O'Malley, H. Millward, D. Eggbeer, R. Williams, R. Cooper, *Addit. Manuf.* **2016**, *9*, 25.

[196] A. Mohammad, M. K. Mohammed, A. M. Alahmari, *Int. J. Adv. Manuf. Technol.* **2016**, *87*, 1033.

[197] W. Wangsgard, M. Winters, *Radiat. Phys. Chem.* **2018**, *143*, 38.

[198] J. M. Beck, M. D. Jacobson, *Minnesota J. Law, Sci. Technol.* **2017**, *18*, 143.

[199] M. Simonelli, Y. Y. Tse, C. Tuck, *Mater. Sci. Eng. A* **2014**, *616*, 1.

[200] M. Simonelli, Y. Y. Tse, C. Tuck, *J. Mater. Res.* **2014**, *29*, 1.

[201] W. Xu, M. Brandt, S. Sun, J. Elambasseril, Q. Liu, K. Latham, K. Xia, M. Qian, *Acta Mater.* **2015**, *85*, 74.

[202] R. Banerjee, S. Nag, S. Samuel, H. L. Fraser, *J. Biomed. Mater. Res. A* **2007**, *81*, 771.

[203] G. Ryan, A. Pandit, D. P. Apatsidis, *Biomaterials* **2006**, *27*, 2651.

[204] J. S. Mulford, S. Babazadeh, N. Mackay, *ANZ J. Surg.* **2016**, *86*, 648.

[205] Y. E. Choonara, L. C. du Toit, P. Kumar, P. P. D. Kondiah, V. Pillay, *Expert Rev. Pharmacoecon. Outcomes Res.* **2016**, *16*, 23.

[206] M. Larsen, R. Mishra, M. Miller, D. Dean, *Bioprinting of Bone*, Elsevier Inc., **2015**.

[207] Y. Oshida, in *Biosci. Bioeng. Titan. Mater.* (Ed.: Y. Oshida), Elsevier, **2013**, pp. 225–268.

[208] M. Puthiya Veettil, J. M. Latham, *Orthop. Trauma* **2015**, DOI 10.1016/j.mporth.2015.02.007.

[209] S. J. Hollister, C. L. Flanagan, D. A. Zopf, R. J. Morrison, H. Nasser, J. J. Patel, E. Ebramzadeh, S. N. Sangiorgio, M. B. Wheeler, G. E. Green, *Ann. Biomed. Eng.* **2015**, *43*, 774.

[210] M. K. Thompson, G. Moroni, T. Vaneker, G. Fadel, R. I. Campbell, I. Gibson, A. Bernard, J. Schulz, P. Graf, B. Ahuja, F. Martina, *CIRP Ann. - Manuf. Technol.* **2016**, *65*, 737.

[211] S. C. Cox, P. Jamshidi, N. M. Eisenstein, M. A. Webber, H. Hassanin, M. M. Attallah, D. E. T. Shepherd, O. Addison, L. M. Grover, *Mater. Sci. Eng. C* **2016**, *64*, 407.

[212] P. S. Unwin, A. Eshraghi, in *Comput. Musculoskelet. Surg. Think. Exec. 3D* (Eds.: L.E. Ritacco, F.E. Milano, E. Chao), Springer International Publishing Switzerland, **2016**, pp.

181–198.

[213] K. C. Wong, *Orthop. Res. Rev.* **2016**, *8*, 57.

[214] R. J. Morrison, K. N. Kashlan, C. L. Flanangan, J. K. Wright, G. E. Green, S. J. Hollister, K. J. Weatherwax, *Clin. Transl. Sci.* **2015**, *8*, 594.

[215] M. Maruthappu, B. Keogh, *Bmj* **2014**, *349*, g7709.

[216] M. Di Prima, J. Coburn, D. Hwang, J. Kelly, A. Khairuzzaman, L. Ricles, *3D Print. Med.* **2015**, *2*, 1.

[217] C. L. Ventola, *P T* **2014**, *39*, 704.

[218] B. Marshall, "Skeletal Wonder From Down Under," can be found under https://www.meddeviceonline.com/doc/skeletal-wonder-from-down-under-0001, **2017**.

[219] T. Economist, "A printed smile," **2016**.

[220] A. Hodgekiss, M. Davies, *Dly. Mail Aust.* **2017**.

Figures and Captions

Figure 1 Examples of customized implants. These implants were designed using 3D Digital Imaging and Communications in Medicine (DICOMs) and fabricated using AM techniques.

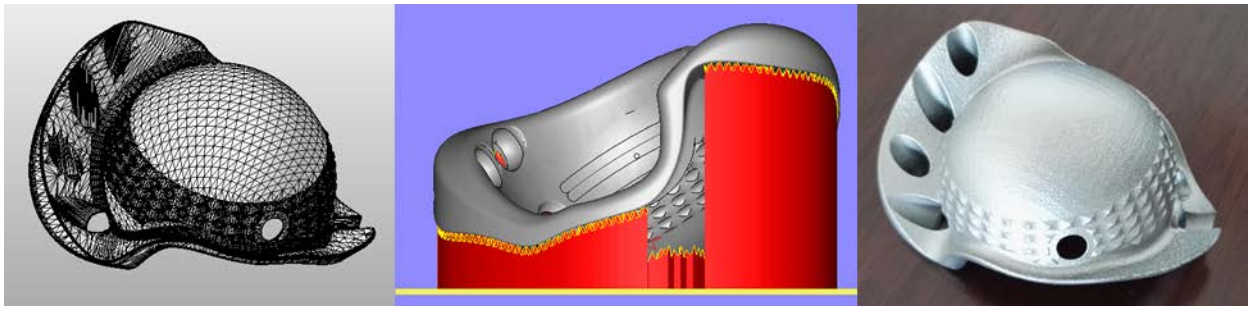

Figure 2 Patient data in the form of computed tomography (CT) scans or magnetic resonance imaging (MRI) scans can be used to create computer aided design (CAD) models, which can then be used to print custom implants. L-R this figure shows the initial design of a custom implant, the pre-print manipulation of the design including support structures in red and the final post-processed part.

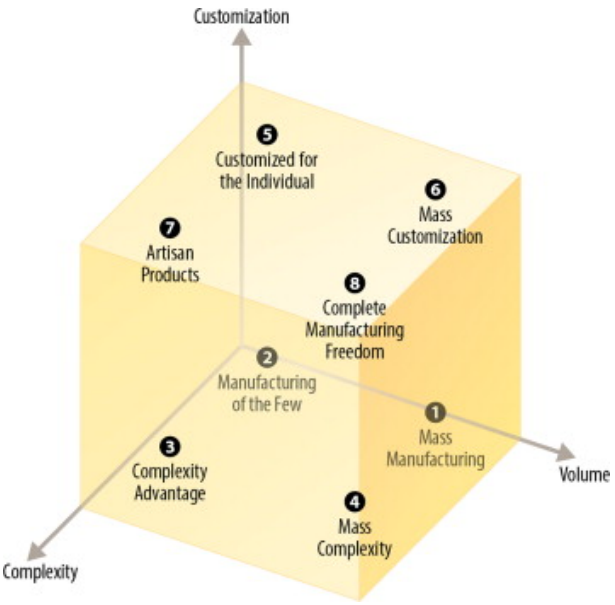

Figure 3 The three-axis model of product manufacturability shows that product design must address complexity, required iterative customizability and required volume to be readily manufacturable.

Reproduced with permission[40] 2014, Elsevier.

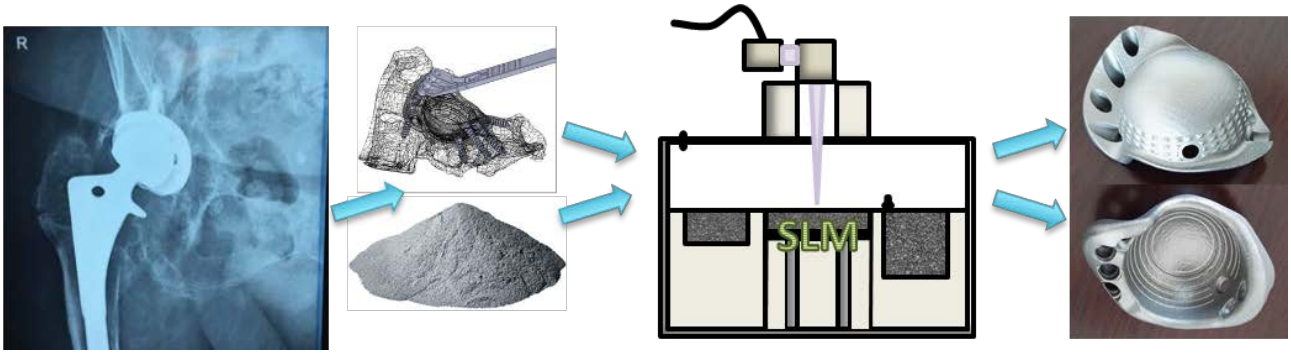

Figure 4 Patients who require custom implants can receive them through the combination of AM techniques and medical imaging. Generally, patient data (e.g. MRI or CT scans) is used to create the design of the part, this CAD file (in stereolithography format) is then sliced and otherwise manipulated such that the AM machine (SLM shown here) can fabricate the part. Following fabrication and some minor post-processing, the custom implant can be delivered to the patient, with a drastically reduced lead time.

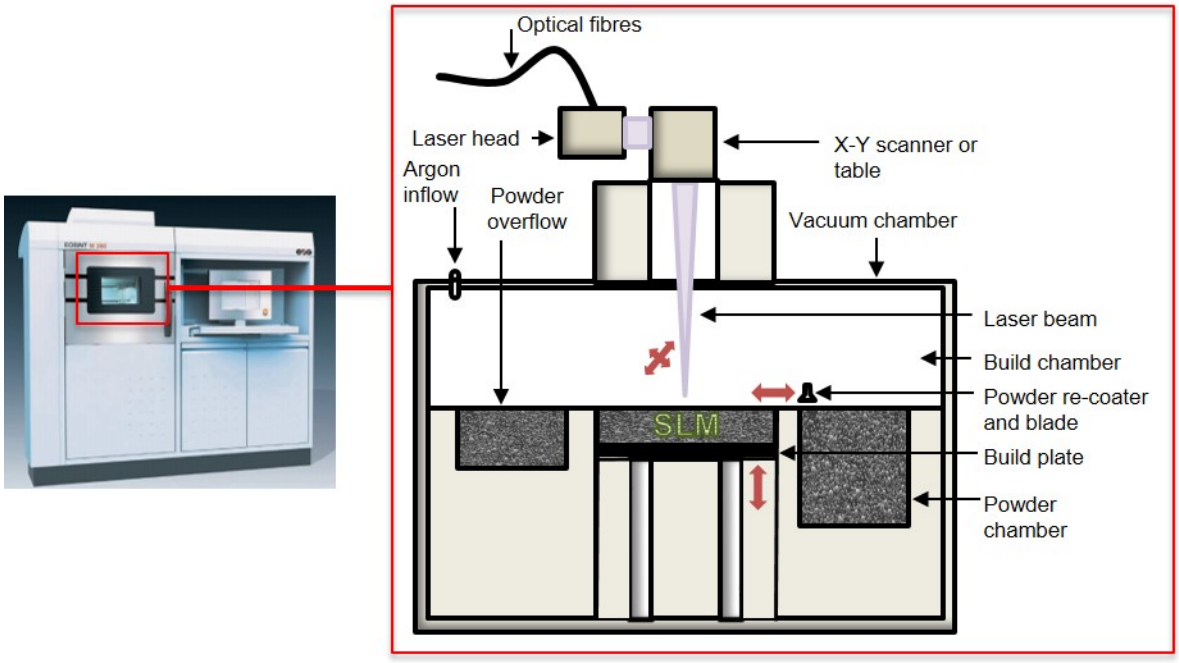

Figure 5 Schematic of SLM Equipment showing fiber laser with, build chamber, powder bunker, powder rake and build-in-progress, and photo of a representative SLM machine.

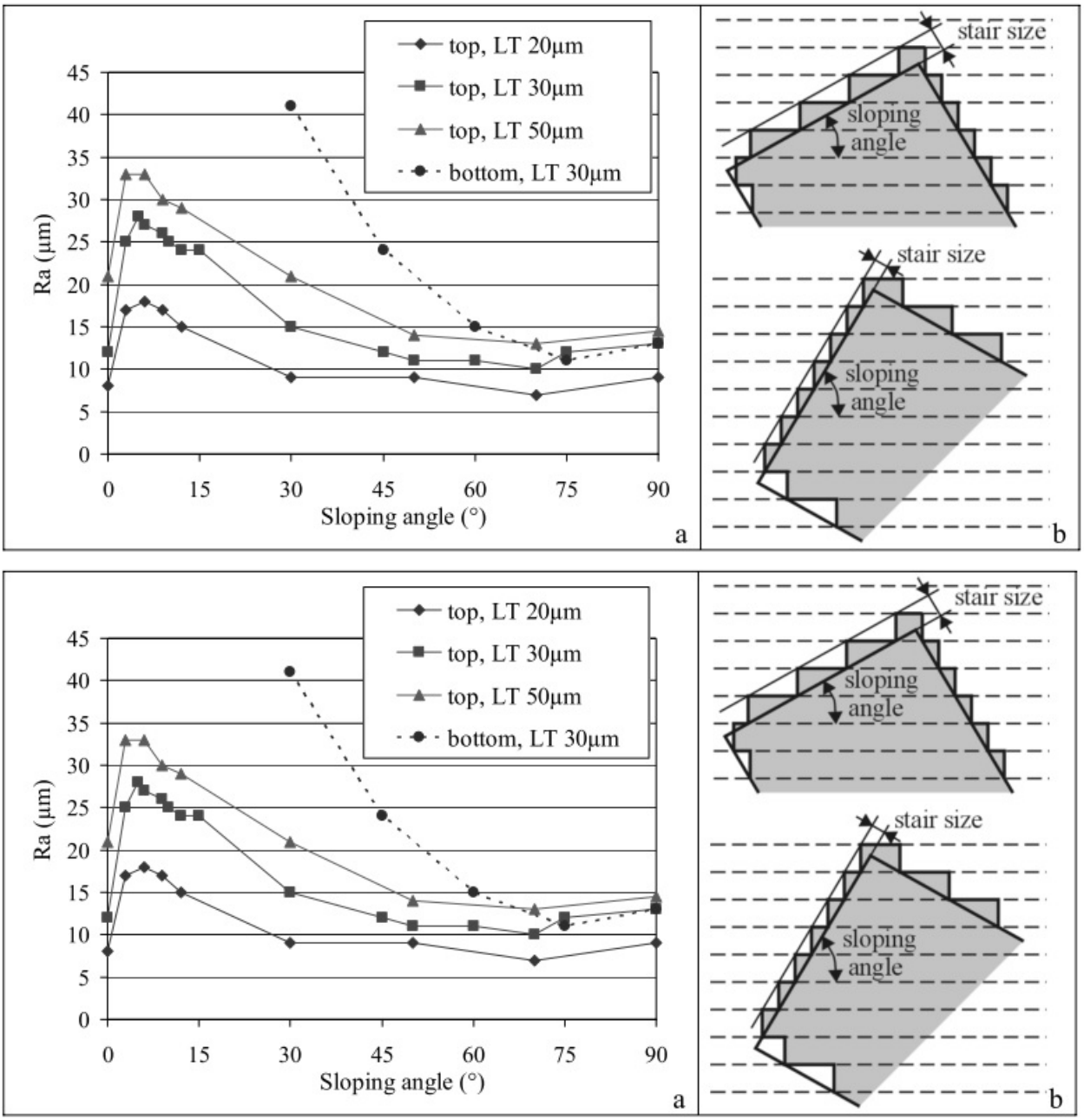

Figure 6 The surface roughness of an SLM produced part can vary significantly according to the surface location when related to a) the printing direction and b) the interaction between sloping angle and layer thickness – 'down-skin' surfaces, or down-facing surfaces show higher surface roughness. This is referred to as the staircase effect.

Reproduced with permission [45] 2007, Elsevier

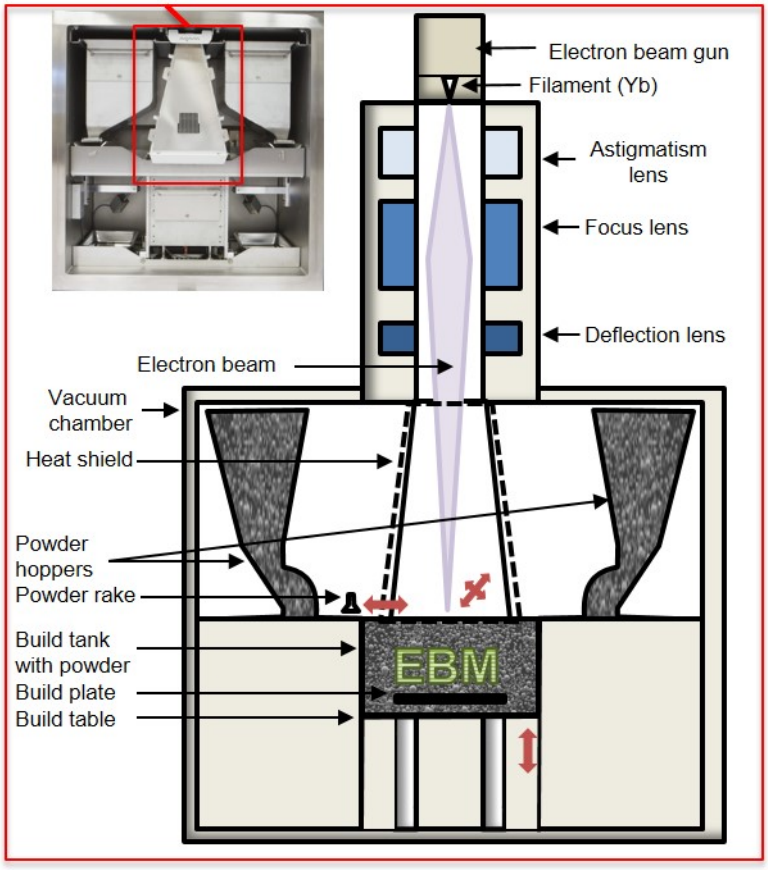

Figure 7 Schematic of EBM machinery showing electron gun assembly, EB focusing lens, EB deflection lens, powder hoppers, powder (layer) rake, build-in-progress, and build table, with photo of representative EBM machine.

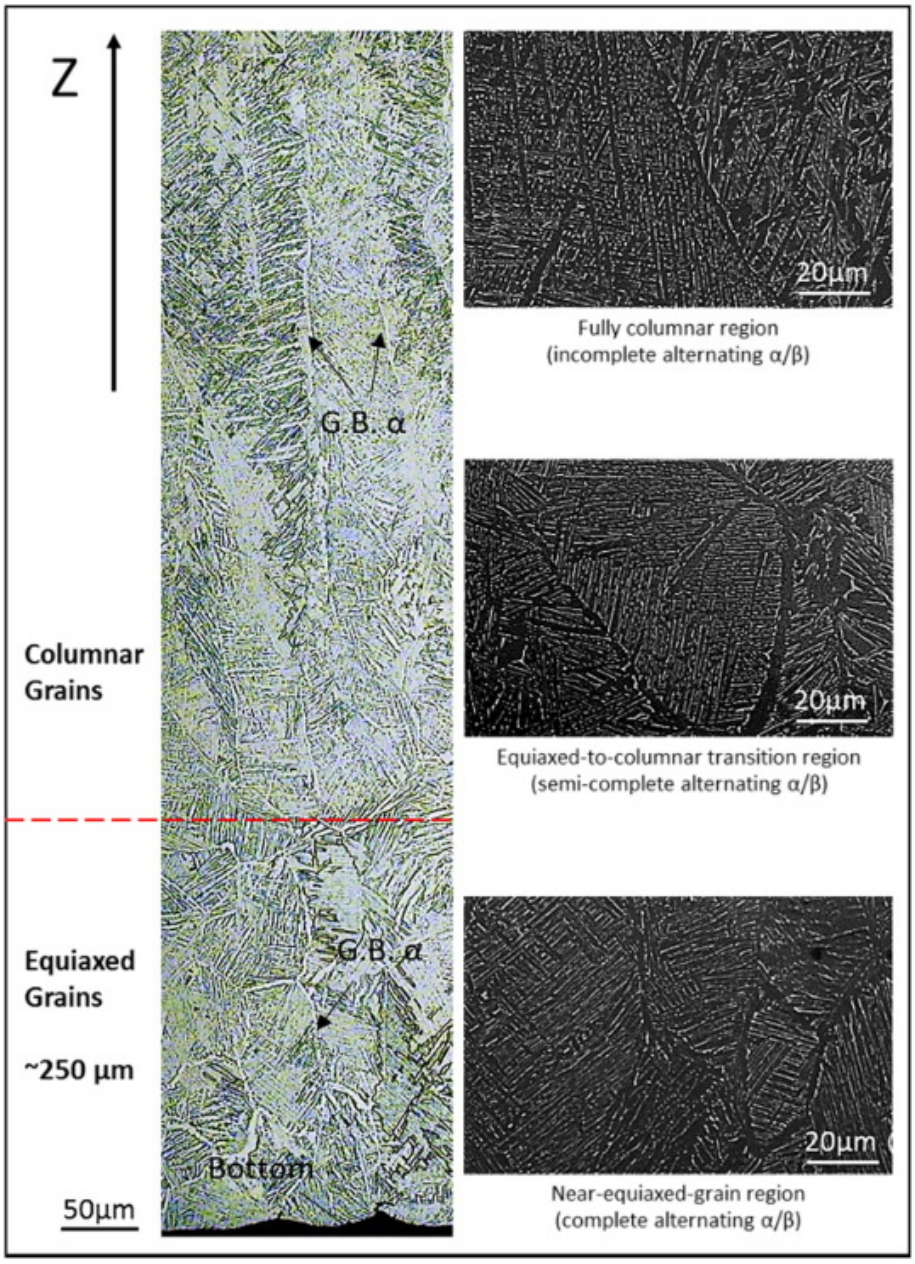

Figure 8 EBM fabrication of Ti-6Al-4V displays an equiaxed to columnar transition of β-grains through the initial 100 layers, with alternating α/β phase evolution as build height increases.

Reproduced with permission [89], 2015, Elsevier

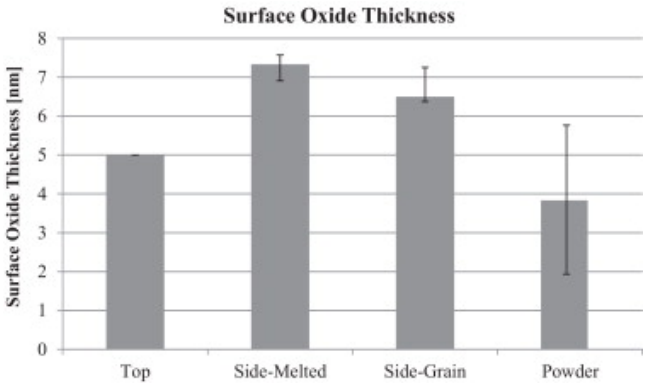

Figure 9 Surface oxide thickness relates to location (i.e. top or side) in EBM fabricated Ti-6Al-4V surfaces, and is related to variations in cooling rates.

Reproduced with permission [91], 2015, Elsevier

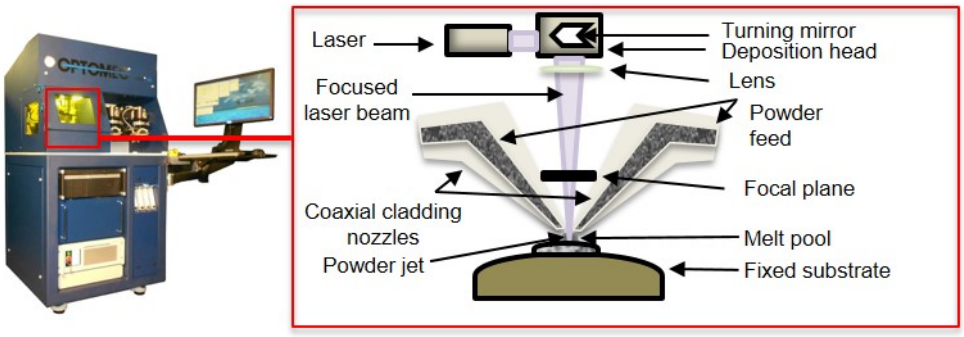

Figure 10 Schematic of DLD machinery showing powder streams converging at the point where they meet the focused laser beam, causing the formation of a melt pool on the fixed substrate, with a photo of a representative DLD machine.

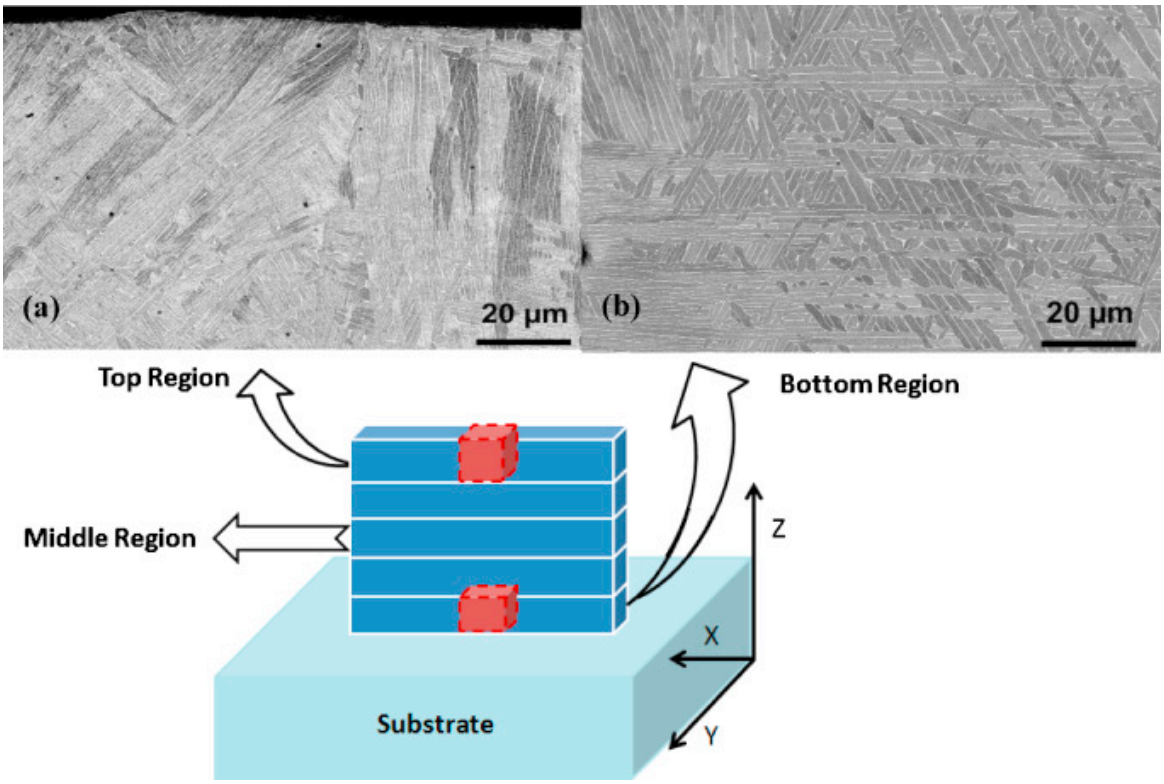

Figure 11 DLD part microstructure changes according to location within the part due to changes in thermal conductivity and repeated heating/cooling cycles, with a) showing the top region and b) showing the bottom region. While both regions display Widmänstatten structures, the top region shows colonies of fine lamellae and large laths, while the bottom region shows comparatively thicker lamellae.

Reproduced with permission [105], 2015, Elsevier

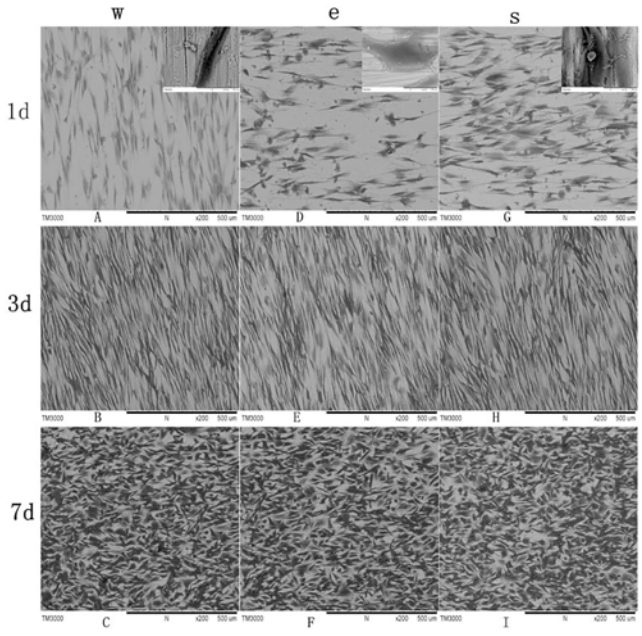

Figure 12 Mesenchymal stem cell seeding on wrought (w), EBM (e) and SLM (s) Ti-6Al-4V samples showing that cell attachment and spreading at all time points was comparable on the EBM and SLM surfaces to the wrought Ti-6Al-4V surfaces (indicating good biocompatibility)

Reproduced with permission [134], 2016, PLOS ONE

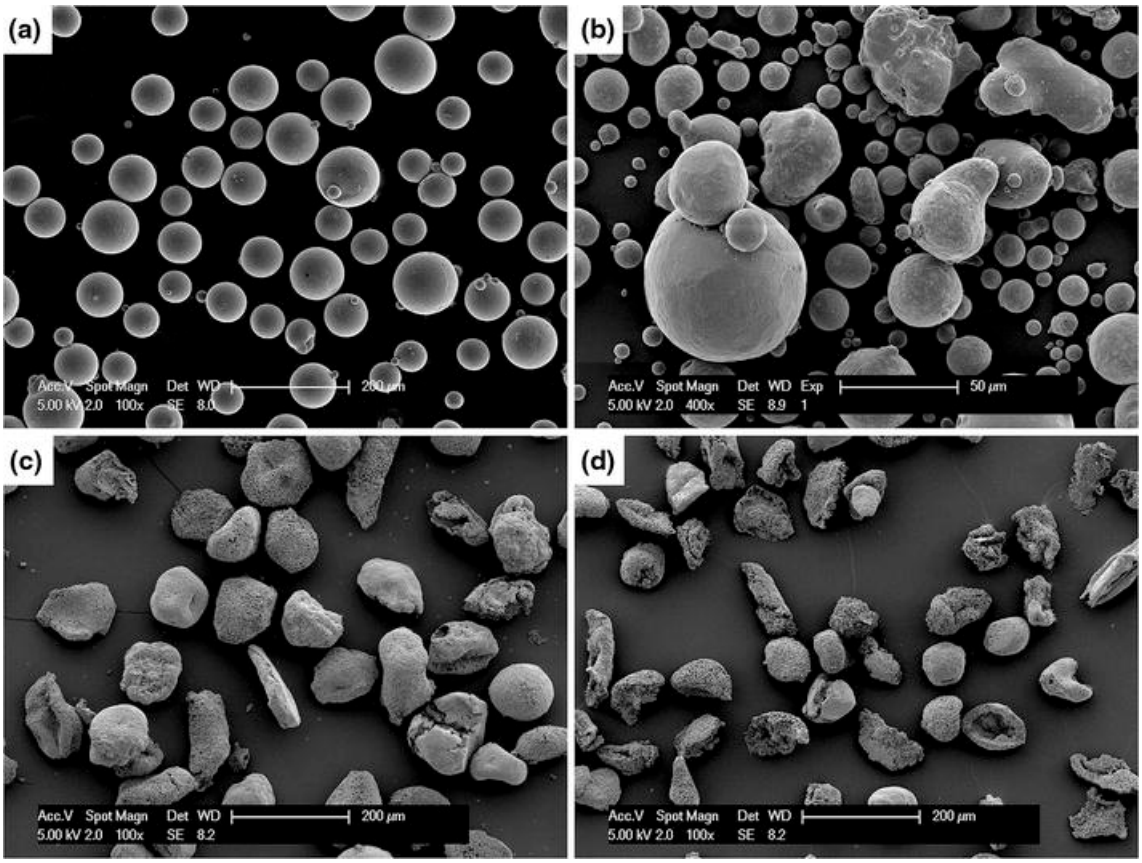

Figure 13 SEM images of a) virgin, b) used Arcam Ti-6Al-4V 45–106 µm powder (undocumented but <30 times), c) 75–106 µm and d) 45–75 µm as-received novel Ti precursor. Different processing and preparation techniques are thus shown to produce vastly different qualities of powder, and thus the choice of feedstock for powder-based AM techniques is of extreme importance.

Reproduced with permission [148], 2015, The Minerals, Metals and Materials Society

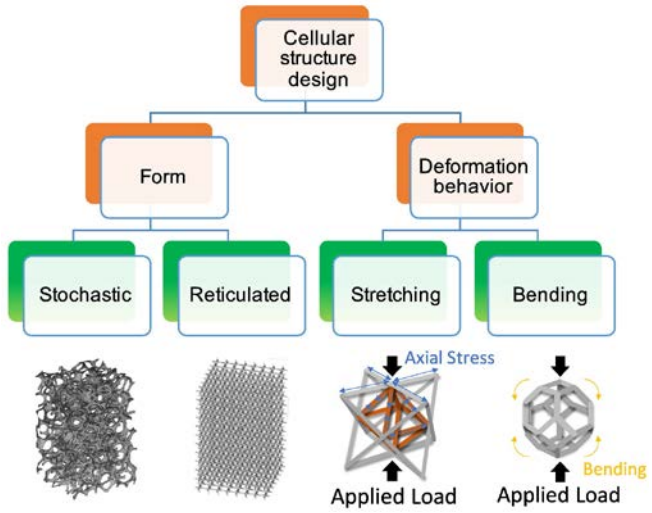

Figure 14 Map of possible cellular scaffold types in terms of form and deformation behavior.

Reproduced with permission [85], 2017, Elsevier

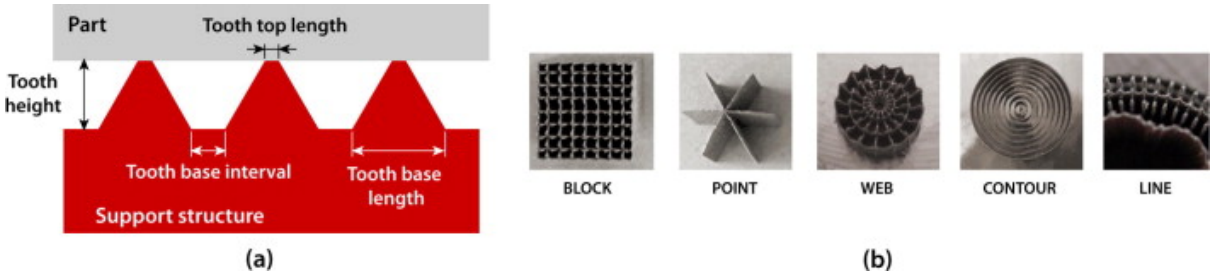

Figure 15 Examples of different types of support structures used for SLM and EBM parts with a) showing tooth characteristics and b) showing alternative support structure designs.

Reproduced with permission [155], 2014, Elsevier

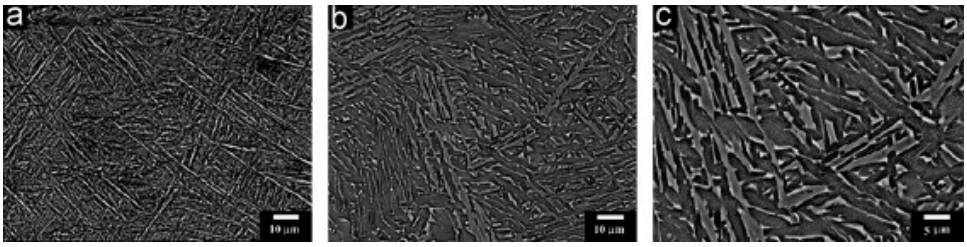

Figure 16 Microstructural changes can be observed according to the different post-processing heat treatment conditions of SLM Ti-6Al-4V, a) shows an SLM sample annealed at 600ºC, b) shows an SLM sample annealed at 700ºC, with α plate formation, and c) shows a HIPed SLM sample.

Reproduced with permission [75], 2013, Elsevier

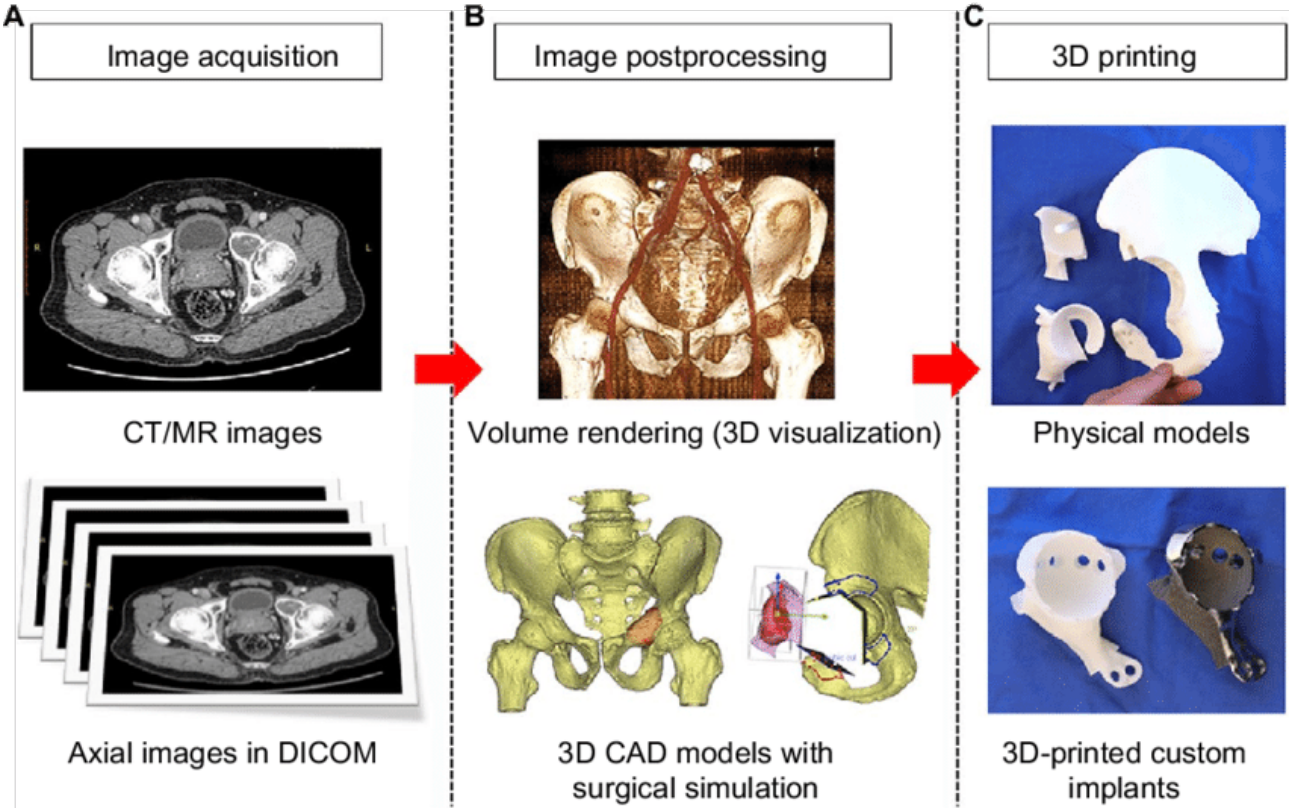

Figure 17 Schematic showing the sequential process of custom implant design and printing showing A) image acquisition, B) image post-processing and CAD modeling, and C) 3D printing of models and custom implants

Reproduced with permission [213], 2016, Dove Press

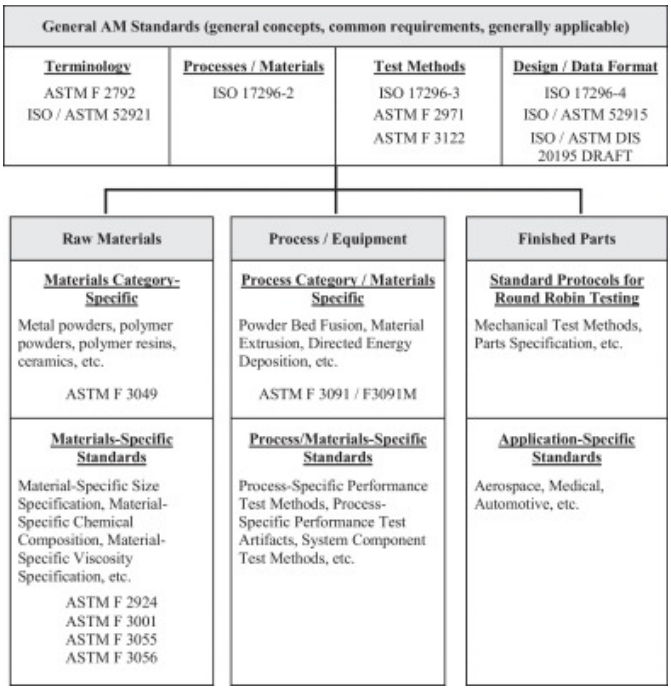

Figure 18 Summary of the ASTM and ISO standards relevant to each stage of producing a customized implant through additive manufacturing.

Reproduced with permission [210], 2016, Elsevier

Table 1. Nominal mechanical properties of common Ti-based alloys used for orthopedic implants [14, 19,20]

Material	Phase types	Fabrication method	Elastic modulus (GPa)	Yield strength (MPa)	Ultimate tensile strength (MPa)	β transus temp-erature (ºC)
Ti-6Al-4V	α + β	Casting	110	850-900	960-970	995
Ti-13Nb-13Zr	α’ + β	Casting	79	900	1030	575
Ti-6Al-7Nb	α + β	Casting	105	921	1024	1010
CP Ti (grade 4)	α	Casting	105	692	100	950
Bone	-	-	10-40	-	90-140	-

Table 2. Selected AM processing parameters and properties of Ti-6Al-4V parts
(N.B. as this table is quite complex, formatting has not been changed to AHM requirements.)

Process	Process parameters						Properties								Ref
	Particle size (µm)	Layer thickness (µm)	Scan rate (mm/s)	Laser power (W)	Spot size (µm)	Hatch spacing (µm)	Young's modulus (GPa)	Yield strength (MPa)	Ultimate tensile strength (MPa)	Elongation (%)	Vickers hardness	Density/ porosity	Surface roughness	Other	
SLM	15-70 (PA*)	50	225	157	70	100	xz; 115±6 zx;119±7 xy; 113±5	xz; 978±5 zx; 967±10 xy; 1075±25	xz; 1143±6 zx; 2228±3 xy; 1199±49	xz; 118±0.5 zx; 8.9±0.4 xy; 7.6±0.5	-	-	upskin – 6.834 sideskin – 28.587 (Ra in µm)		[199]
	15-75 (PA*)	50	58	42	30	30	119±7	-	-	-	500	99.4±0.2%	-		[200]
	5-50 (PA*)	30	1600	250	52	60	109±7	967±10	1117±3	8.9±0.4	-	-	-		[161]
	30 (GA**)	50	200	200	130	50	-	910±9.9	1035±29.0	3.3±0.76	-	-	-		[98]
	15-25 (GA**)	30 60 90	686 710 102	175 375	-	12 18	-	1100	-	-	-	-	-		[201]
	20-50 (GA**)	20	800-1500	150-200	150	75	-	>1 (0.2% proof stress)	1200	<10	-	0.1%	-		
	43 (GA**)	30	710	175	-	150	-	-	-	-	-	-	-		[51]
	40	30	450	100	-	-	-	1008±30	1080±30	1.6±2%	-	-	-	mean fatigue life of 27,000 cycles	[52]
EBM	30 (GA**)	build parameters absent						1150	1200	25%	3.6 3.8 3.6			for EBM1 (top end)	
								1100	1150	16%	4.1			for EBM2 (top end)	
								1170	1230	12%	380			for	

Process	Process parameters						Properties								Ref
	Particle size (µm)	**Layer thickness (µm)**	**Scan rate (mm/s)**	**Laser power (W)**	**Spot size (µm)**	**Hatch spacing (µm)**	**Young's modulus (GPa)**	**Yield strength (MPa)**	**Ultimate tensile strength (MPa)**	**Elongation (%)**	**Vickers hardness**	**Density/ porosity**	**Surface roughness**	**Other**	
														wrought Ti64	
	Table d45-100 (GA**)	70	Arcam standard	60 kV	Arcam standard	Arcam standard	180±15				425±50				[36]
	45-100 (GA**)	100	energy input per unit length = 0.55 J/mm, line offset of 1.0 mm				parallel loading = 12.9±0.9 perpendicular loading = 3.9±2.1 complete infiltration of osseous tissue	parallel loading =148.4±3.5 perpendicular loading =127.1±29.2				mean pore size = 0.45 mm porosity = 61.3%		designed porosity	[86]
	45-105	50	arcam standard	arcam standard	arcam standard	arcam standard		top layer =823.4±0.1 bottom layer =851.8±5.8	top layer =940.5±6.5 bottom layer =964.5±0.3	top layer =13.2±0.7 bottom layer =16.3±0.8	top layer =319±5, bottom layer =327±5	-	-		[89]
	45-105	50						10 mm 1; 851.8±5.8 10 mm 2; 836.6±8.7 10 mm 3; 827.9±0.9 10 mm 4; 823.4±0.1	10 mm 1; 964.5±0.3 10 mm 2; 953.7±4.3 10 mm 3; 944.5±5.8 10 mm 4; 940.5±6.5	10 mm 1; 16.3±0.8 10 mm 2; 15.2±1.2 10 mm 3; 14.0±0.5 10 mm 4; 13.2±0.7					
DLD	50-150	-	22.5 mm/s	200 W	-	-						30%			[108]
	150 mesh	-	635 mm/min	350 W	-	hatch distance of 0.38 mm, with layer spacing of 0.25 mm								single β phase formed, average grain size of 50 µm	[202]

Process	Process parameters						Properties								Ref
	Particle size (µm)	Layer thickness (µm)	Scan rate (mm/s)	Laser power (W)	Spot size (µm)	Hatch spacing (µm)	Young's modulus (GPa)	Yield strength (MPa)	Ultimate tensile strength (MPa)	Elongation (%)	Vickers hardness	Density/ porosity	Surface roughness	Other	
	45	30	1250	170	100	-	-	1185	1293	6.23	402.81±11.31	-	35±5	-	[119]
	15-45	50	EOS default	EOS default	100	-	114.9	1093	1130	-	-	95-99% dense	11-13	-	[46]
	(GA**)	30	0.6 m/min, powder feed rate = 1 g/min	330	-	50	-	1005	1073	4	-	-	-		[133]
	89 (PREP†)		10.6	2 kW	-	-	111±3	938±22	1048±23	23±3					

* Plasma atomized particles
** Gas atomized particles
† Plasma rotating electrode process used to prepare particles

Author Biographies;

Trina Majumdar

Trina Majumdar received her BE and BBiomedSci in materials engineering from Monash University in 2014 and is currently a 3rd year Ph.D. candidate in the Birbilis group at the Materials Science and Engineering department at Monash University. Her doctoral research under the supervision of Prof. Nick Birbilis examines the additive manufacturing of titanium based orthopedic implants, with a focus on the manipulation of additive manufacturing process parameters to produce implants with improved osseointegrative capabilities.

Sophie Cox

Dr Sophie C. Cox is a Lecturer in the School of Chemical Engineering working within the Tissue Regeneration And Interfaces Lab (TRAILab). Her research focuses on the design of biomaterials and manufacturing methods that maximize regeneration of damaged or diseased tissue. She is particularly interested in the relationship between biomaterial properties and biological response as well as the development of additive manufacturing techniques to fabricate medical implants.

Nick Birbilis

Professor Nick Birbilis is the Head of Materials Science and Engineering at Monash University and the Woodside Innovation Chair. His research spans the broad areas of metallurgy, corrosion and corrosion control. He is a Fellow of NACE and the Electrochemical Society.

Table of Contents Entry;

The use of additive manufacturing for the low-cost, fast lead-time manufacturing of customized orthopedic implants is becoming rapidly more feasible. The three major techniques used are selective laser melting (SLM), electron beam melting (EBM) and direct laser deposition (DLD). This review presents a timely examination of the current state of the art in each of these techniques, with a focus on the implant properties achievable by each technique. The issues that must be considered prior to and following fabrication are summarized, and the review ends with a consideration of the bench to bedside perspectives.

Keyword: Additive manufacturing

Authors: Trina Majumdar, Jess E. Frith, Neil Eisenstein, Sophie C. Cox, Nick Birbilis*
Title: Additive Manufacturing of Titanium Alloys for Orthopedic Applications: A Materials Science Viewpoint

ToC figure, 110 mm broad × 20 mm high: